UNCERTAINTY QUANTIFICATION OF THE HOMOGENEITY OF GRANULAR MATERIALS THROUGH DISCRETE ELEMENT MODELING AND X-RAY COMPUTED TOMOGRAPHY

A Thesis

by

PATRICK RUSSELL NOBLE

Submitted to the Office of Graduate Studies of
Texas A&M University
in partial fulfillment of the requirements for the degree of

MASTER OF SCIENCE

August 2012

Major Subject: Civil Engineering

UNCERTAINTY QUANTIFICATION OF THE HOMOGENEITY OF GRANULAR MATERIALS THROUGH DISCRETE ELEMENT MODELING AND X-RAY COMPUTED TOMOGRAPHY

A Thesis

by

PATRICK RUSSELL NOBLE

Submitted to the Office of Graduate Studies of
Texas A&M University
in partial fulfillment of the requirements for the degree of

MASTER OF SCIENCE

Approved by:

Chair of Committee,	Zenon Medina-Cetina
Committee Members,	Rashid Abu al-Rub
	Ozden Ochoa
Head of Department,	John Niedzwecki

August 2012

Major Subject: Civil Engineering

ABSTRACT

Uncertainty Quantification of the Homogeneity of Granular Materials through Discrete Element Modeling and X-Ray Computed Tomography. (August 2012)

Patrick Russell Noble, B.S., Texas A&M University

Chair of Advisory Committee: Dr. Zenon Medina-Cetina

Previous research has shown that the sample preparation method used to reconstitute specimens for granular materials can have a significant impact on its mechanistic behavior. As the Discrete Element Method becomes a more popular choice for modeling multiphysics problems involving granular materials, the sample heterogeneity should be correctly characterized in order to obtain accurate results. In order to capture the effect of sample preparation on the homogeneity of the sample, standard procedures were used to reconstitute samples composed of a homogeneous granular material. X-ray computed tomography and image analysis techniques were then used to characterize the spatial heterogeneity of a typical sample. The sample preparation method was modeled numerically using the Discrete Element program PFC3D. The resulting microstructure of the numerical sample was compared to the results of the image analysis to determine if the heterogeneity of the sample could be reproduced correctly for use in Discrete Element Modeling.

ACKNOWLEDGEMENTS

First, I would like to thank my advisor and Committee Chair for his patience, guidance, and support on this work. Without his advice and guidance this work would not be possible. It has truly been a pleasure to work with him on this fascinating topic. I have learned many lessons to be applied not only while working with others on a research project, but also in life, from his experience and leadership.

I would also like to thank my parents, family, and friends for their constant support and encouragement. Without their support I would not be the person that I am today.

I would like to thank Tam Doung and Emad Kassem for helping perform the experimental portions of this work, including performing the CT scans, preparing samples, and running numerical models.

I also appreciate all of the help from David Potyondy and ITASCA for their help and guidance with PFC3D and the use of a license.

I also appreciate all the guidance from Mike Linger and Sammy Priano for helping to set up and fabricate the required laboratory equipment needed for this research project.

TABLE OF CONTENTS

CHAPTER Page

LIST OF FIGURES

LIST OF TABLES

CHAPTER I

INTRODUCTION

In recent years the Discrete Element Method (DEM) has become a popular tool for modeling the behavior of granular materials. The Discrete Element Method allows the user to model a discontinuous media, such as soils or sands, to capture localized deformation during loading. DEM was originally conceived by Cundall and Strack in the 1970's [1]. DEM simulations have been used to simulate a wide spectrum of engineering applications, such as the modeling of granular flow through a hopper [2], the behavior of aggregates serving as railway ballast [3], the microstructural response of asphalt [4], and rock mechanics [5]. One limiting factor to DEM analysis is the fact that true grains are rarely spherical in shape, thus interlocking between grains cannot be captured. To overcome this limitation, researchers have investigated techniques to accurately capture particle shapes and implement these shapes into DEMs by using clumped spheres, tetrahedral elements, ellipsoidal elements, spherical harmonics, and digital image acquisition [6-11]. As DEM analysis becomes more prevalent, it can be used to model multi-physics problems. For example, the Discrete Element Method has already been used to model the disturbance of soil columns due to fluid flow [12]. As these more complicated models become more prevalent, the heterogeneity of samples tested numerically should be accurately introduced since it has been shown that specimen heterogeneity affects material behavior under shearing.

This thesis follows the style of *Computers and Geotechnics*.

1.1 Literature Review on Sample Preparation

Viad et al. [13] reconstituted Fraser River sand samples using the water pluviation and moist tamping techniques. Even though samples created using different techniques had nearly identical void ratios, the behavior of the samples varied greatly depending on the preparation method for both triaxial compression and extension tests. Samples prepared with the moist tamped technique showed a liquefaction behavior, while samples prepared with the water pluviation method showed a dilative behavior. Viad et al. also examined the response of undisturbed undrained sand specimens to determine if the sample preparation technique affected the behavior of the samples. The undisturbed samples exhibited the same behavior as the reconstituted water pluviation sample and had nearly identical void ratios. Due to the behavior of the samples, Viad et al. recommends the water pluviation method for reconstituting sand specimens over the moist tamped technique. However, Viad et al. [13], does acknowledge that the friction angle was essentially the same for samples reconstituted using both methods.

Yamamuro et al. [14] also compared the behavior of sand/silt specimens under various reconstitution techniques including: slurry deposition, air pluviation, water pluviation and the dry funnel deposition method. Specimens were composed of Nevada sand with varying levels of silt content. It was determined that the difference in behavior was a result in the difference in the soil fabric of the samples generated using different techniques. After placing specimen sections under a scanning electron microscope, samples generated using the dry funnel deposition method had less stable grain to grain contacts which resulted in these samples undergoing temporary

liquefaction under shearing, while pluviated samples had more stable grain contacts which resulted in a stable response. Yammamuro et al. [14] defined a stable grain contact as a contact between large-to-large grains, while an unstable contact formed when large, small, and large grains came into contact with each other. Grain contacts were determined by sanding the surface of various sections in 20 micrometer intervals. Six layers were taken from each sample to verify the grain contact and the size of the grains in contact with each other. Grains were numbered in four alternating slices, and the number of contacts for each grain was determined. Figure 1 compares the percentage of stable and unstable contacts for two sand specimens.

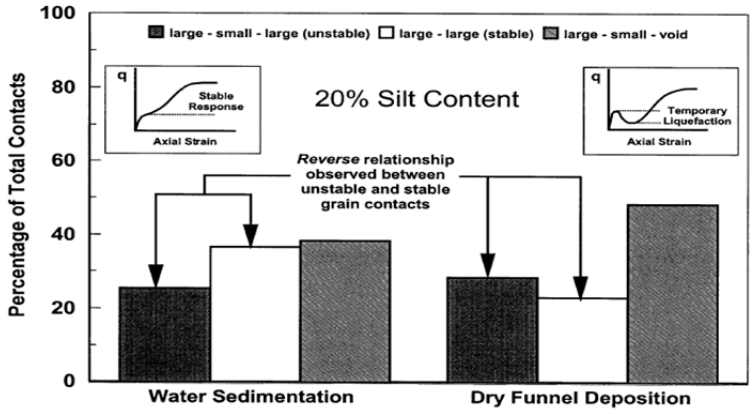

Figure 1: Comparison of Stable and Unstable Grain Contacts [14].

Thomson and Wong [15] also showed that the water pluviation and moist tamped reconstitution methods resulted in non-homogeneous samples. Samples prepared by the water pluviation method were fairly homogeneous with only the top quarter of the sample having a lower void ratio than the rest of the sample. While samples prepared

with the moist tamped method were fairly non-homogeneous as the void ratio varied within each tamped layer of the sample. It has been proposed to under- compact the first layers while using the moist tamped procedure so that when the final layer is deposited, the void ratio will be the same throughout the sample. However it is difficult to under-compact each layer correctly so that the end result will have the desired final density. The void ratio distributions were also studied while the samples were undergoing compression. At high compression levels the void ratio of both the moist tamped and water pluviated samples became more uniform. Thomson and Wong state that the effect of the void ratio on the global behavior of specimens is of interest and that the variation of the void ratio should continue to be evaluated. Figure 2 compares the initial slice mean void ratios of two reconstituted sand specimens.

Monkul [16] showed that the densification technique, either tamping or tapping, also contributed to increase the strength behavior of undrained sand specimens. Monkul prepared samples with the funnel deposition method and the moist tamping method. Densification can be achieved when using the funnel deposition method by either tapping the mold while the sample is being deposited, by increasing the speed at which the funnel is raised through the mold, or by increasing the length of a tube attached to the end of the funnel. Monkul [16] showed that specimens prepared with different techniques would result in different peak stress values even though the overall density of each sample was similar.

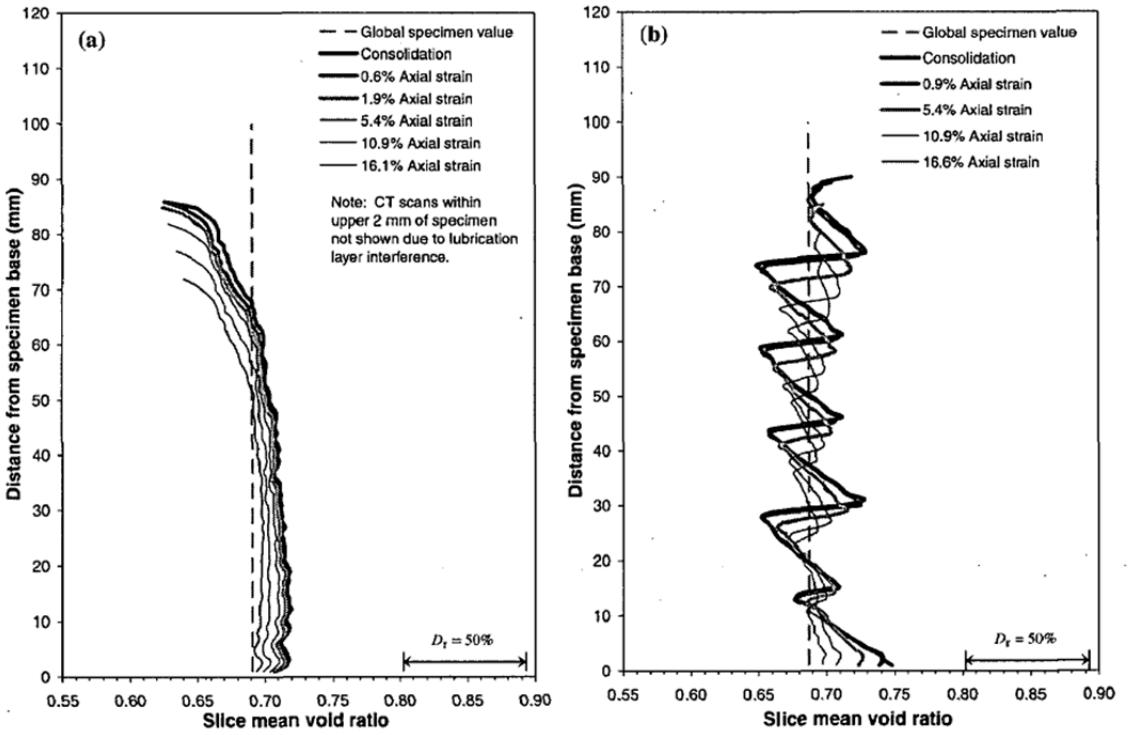

Figure 2: Comparison of Void Ratios for a Water Sedimentation and Moist Tamped Sand Sample [15].

Jiang et al. [17] developed an algorithm for generating homogeneous packings of particles for use in the Discrete Element Method. Jiang et al. also discussed current techniques used for generating homogeneous specimens such as the isotropic-compression method and expansion method. The isotropic-compression method developed by Cundall [1] randomly places particles in a predetermined area. The particles are not allowed to overlap each other to prevent excessive contact forces to develop while the sample is being formed. The friction contact coefficient between all the particles is then reduced, while the bounding walls collapse to increase the sample density. After a target void ratio is reached, the walls come to rest and the original

friction coefficient is reestablished. The expansion method employed by PFC3D also begins by random placing particles so that they cannot overlap each other, however the radius of the particles is reduced so that the required number of particles needed to reach the target void ratio can be generated at once. After all of the particles are generated, the friction coefficient is reduced, and the radius of each particle is increased to the desired value. After the particles come to rest, the friction coefficient is restored. The algorithm developed by Jiang et al [17], involves generating particles in multiple levels. Each level is then compacted until the target void ratio is reached. In order to avoid over compaction of the bottom layer, the bottom layers are under compacted so that the final density is uniform.

Fu et al. [18] investigated the packing of pharmaceutical powders using x-ray microtomography and the Discrete Element Method. Fu et al. studied the deposition of glass beads and cellulose. Samples were prepared by pouring the spheres into a three millimeter tube with the use of a paper funnel. The DEM simulation formulated involved using 2000 spherical particles to represent the non spherical material. The spheres were dropped from a given height and allowed to settle under gravity in a rectangular box. The packing fraction and RDF measurements were used to compare the reconstructed 3D images and the DEM models. The DEM simulations showed good agreement with the images for both the packing fraction and RDF calculations.

1.2 Problem Formulation

Due to differences in the microstructure of reconstituted samples that contributes to the failure mechanism of granular materials, a method for accurately describing

specimen heterogeneity is for use in the Discrete Element Model is introduced. Sample heterogeneity is determined by first generating samples of a homogeneous granular material using standardized techniques that are used to reconstitute homogeneous specimens. CT scans of a typical sample were taken and analyzed using MATLAB [19] to determine the variation in the spatial distribution of particles throughout the sample. The spatial heterogeneity of the sample is described by the planar void ratio along the height of the specimen and throughout the surface of each slice in this work. The sample preparation techniques are also modeled numerically using the Discrete Element Method to determine if this process can inherently introduce the sample heterogeneity. Using the positions of the spheres from the numerical model, slices are generated to compare the heterogeneity of the numerical sample with the experimental results.

CHAPTER II

SAMPLE PREPARATION

Multiple methods currently exist to reconstitute soil and sand specimens for geotechnical experiments as discussed in the literature review. The air pluviation and dry funnel deposition method were employed for this project to produce samples of the densest and loosest condition respectively. These methods were chosen since they are commonly used to create homogenous specimens at different densities.

2.1 Granular Material

Thomson precision chrome steel ball bearings were chosen as the granular material for this study. This material was chosen since each sphere is nearly identical and fabricated to within tight tolerances. This same material has previously been used by researchers such as O'Sullivan and Cui to calibrate Discrete Element Models [20]. The application of a single grain distribution allows for multiple parameters to be controlled in this study. The shape, angularity, and texture of the grains are kept constant and directly match the characteristics of the particles in the numerical model. Three millimeter and six millimeter diameter spheres were used for reconstituting specimens following the methods described as follows. The six-millimeter spheres were used to make comparisons with the numerical results, since larger particles would decrease the computational requirements for the numerical models.

The density of the material is an important parameter for determining the global void ratio of the samples prepared in the lab, as well as for calculating forces imparted

on particles in the discrete element model. The density of the steel was obtained by measuring the weight of a set number of spheres. 100 spheres were randomly selected from the material population and were weighed. With a known particle diameter, the total volume of material could be calculated as well as the density of the material. This experiment was conducted five times to obtain an average density of 7,830 kg/m^3. This agrees closely with the density of 7,800 kg/m^3 obtained by O'Sullivan and Cui [20].

2.2 Air Pluviation Method

The air pluviation method used in this project was performed as follows. Two sieves, one with an 8 mm opening and the other with a 3.35 mm opening, were placed at the top of a tube that had the same diameter as a split mold used to hold the material in place. The sieves were used to evenly disperse the material as it was deposited at the top of the tube and were chosen since the maximum diameter of the steel spheres is three millimeters. The 3.35 mm opening sieve was removed while preparing specimens using the six-millimeter spheres. The test apparatus was prepared by first attaching a 72 mm diameter membrane to the base of the triaxial cell. Two o-rings were used to hold the membrane in place and ensure a tight seal with the base of the split mold. A 72 mm x 136 mm split mold was then placed around the membrane and secured in place with the use of two hoop clamps. One hoop clamp was placed at the bottom of the mold to apply direct pressure on the o-rings securing the membrane. The second hoop clamp was placed at the top of the mold to close the vertical seams along the mold. Without this arrangement of clamps and o-rings, a proper seal could not be generated and the membrane would not adhere to the sides of the mold. After the membrane was stretched

around the top of the mold, vacuum pressure was applied to the mold to hold the membrane in place while the sample was prepared. An aluminum cap was then placed on the mold to allow the pluviation tube to be secured to the split mold. By using this arrangement, the tube was ensured to remain vertical and remain in place during testing. The height of the pluviation tube could be altered by attaching varying pieces of six-inch lengths. Images describing the sample preparation methods can be found in Appendix A (Figure 47 through Figure 55).

Approximately 3000 grams of material were placed in a funnel to ensure that the entire sample would be deposited in one layer. Great care was taken to ensure that the funnel was held above the center of the sieves. The granular material was then released from the funnel, rained down from the top of the sieves through the tube and into the split mold. After the tube was removed from the mold, excess material was removed by running a steel ruler over the top of the split mold. One pass of the steel ruler was made during each test to remove any subjective decision as to when a sphere was considered outside of the mold. No spheres were replaced in the voids generated in the top of the mold after removing the excess material. After securing the porous stone and top cap to the sample with another set of o-rings, vacuum pressure was applied to the base of the sample and the split mold was removed.

2.3 Void Ratio Determination

Six measurements of the specimen diameter and three measurements of the sample height were made with the use of digital calipers. The void ratio of each sample was determined by the following formula:

$$e = \frac{V_v}{V_S}$$

where e is the void ratio, V_v is the volume of voids and V_S is the volume of solids. The total volume of the sample was calculated by taking the average diameter and height of the specimen. The volume of solids was found by multiplying the weight of the sample by the density of the steel, and the volume of voids was found by subtracting the volume of solids from the total volume. The length of the tube was varied in increments of six inches from zero inches (sieves directly on the mold) to three feet to produce specimens with varying densities. Each experiment was performed ten times at each drop height to determine the repeatability and the inherent variability of the experiment.

2.4 Funnel Deposition Method

The loosest condition was achieved by implementing the funnel deposition method. This technique was performed by attaching a tube to the bottom of a funnel. This apparatus was then placed in the center of the split mold, which was prepared in the same fashion as stated above. The length of the tube was determined by the size of the split mold. The steel ball bearings were then placed inside the funnel and allowed to settle through the tube. The tube/funnel apparatus was then slowly raised along the center of the mold. This effectively allowed the spheres to be deposited in the mold with zero drop height. The void ratio was then calculated for each sample in the same manner

as stated above. Ten experiments were also performed for the funnel deposition method. Various figures explaining the sample preparation process can be found in Appendix A.

2.5 Results

The results for samples comprised of three-millimeter spheres can be seen in Figure 3 and Figure 4, and results for samples comprised of six-millimeter spheres can be seen in Figure **5** and Figure 6. From these figures it can be observed that the void ratio decreased and the sample weight increased as the drop height increased. The drop height was measured from the base of the sample to the mesh of the lowest sieve. The funnel deposition method generated the loosest condition. The air pluviation method produces specimens with a higher density due to the increase in the amount of energy imparted on the particles due to gravity as they rain down the pluviation tube. As the mold is filled with material, the raining particles impact the spheres below compacting the specimen and reducing voids.

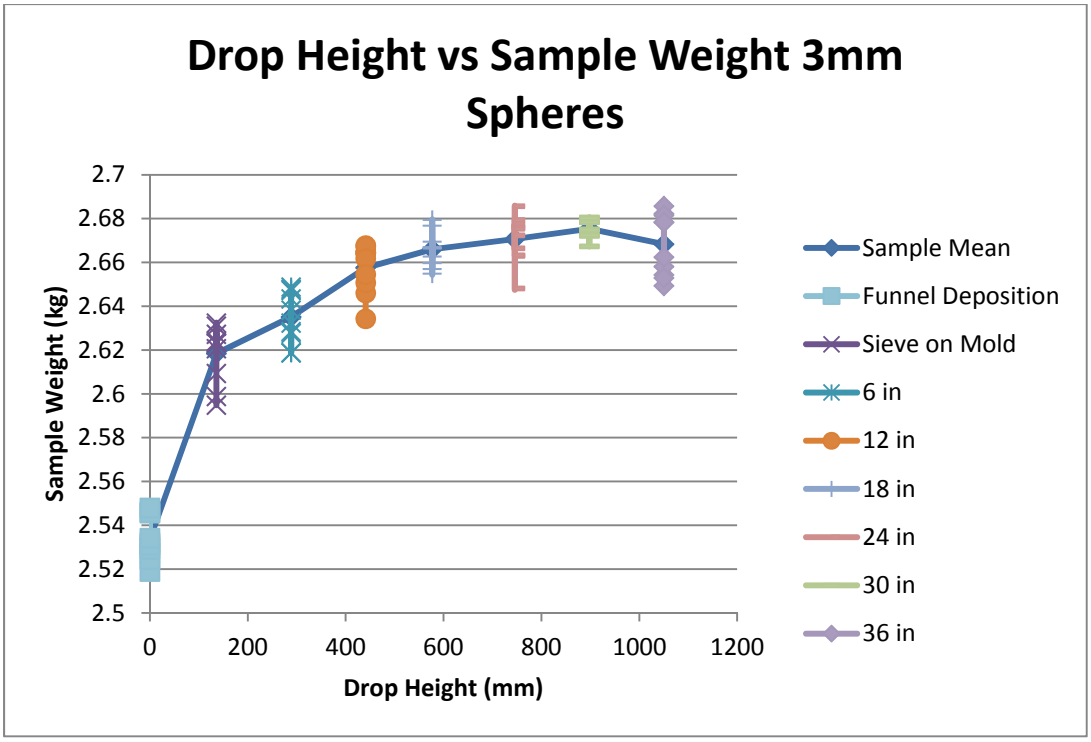

Figure 3: Drop Height vs. Sample Weight for 3mm Sphere Samples

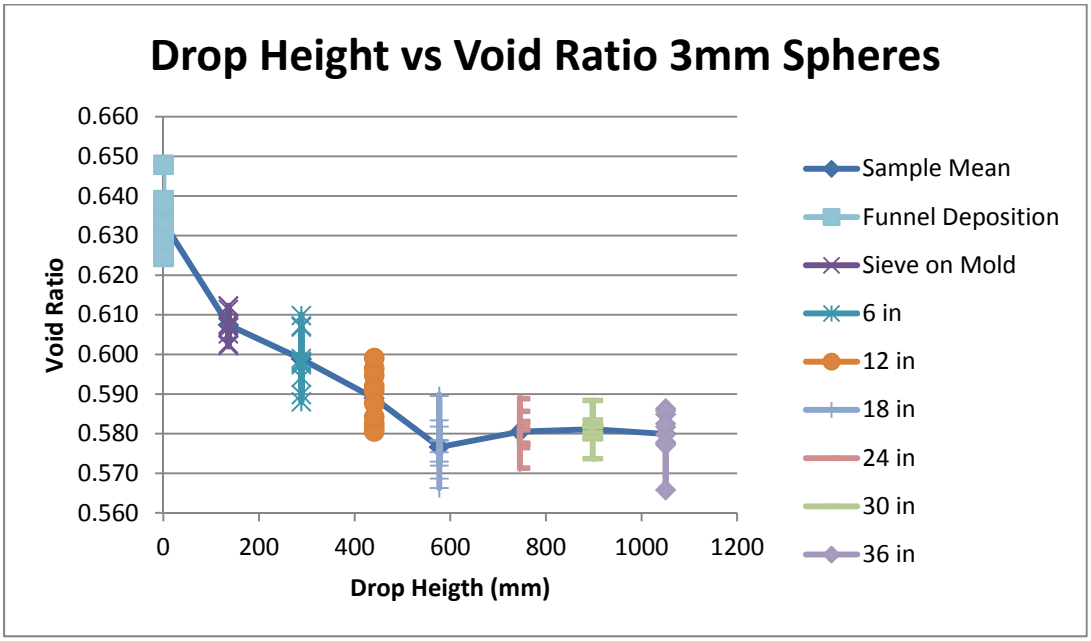

Figure 4: Drop Height vs. Void Ratio for 3mm Sphere Samples.

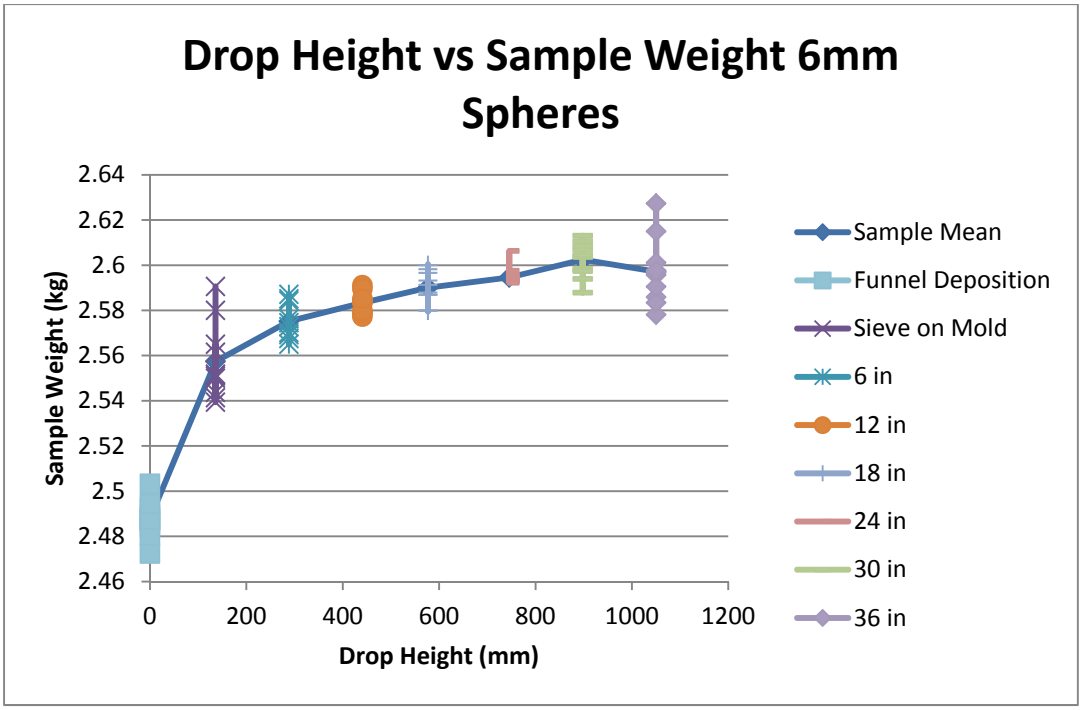

Figure 5: Drop Height vs. Sample Weight for 6mm Sphere Samples

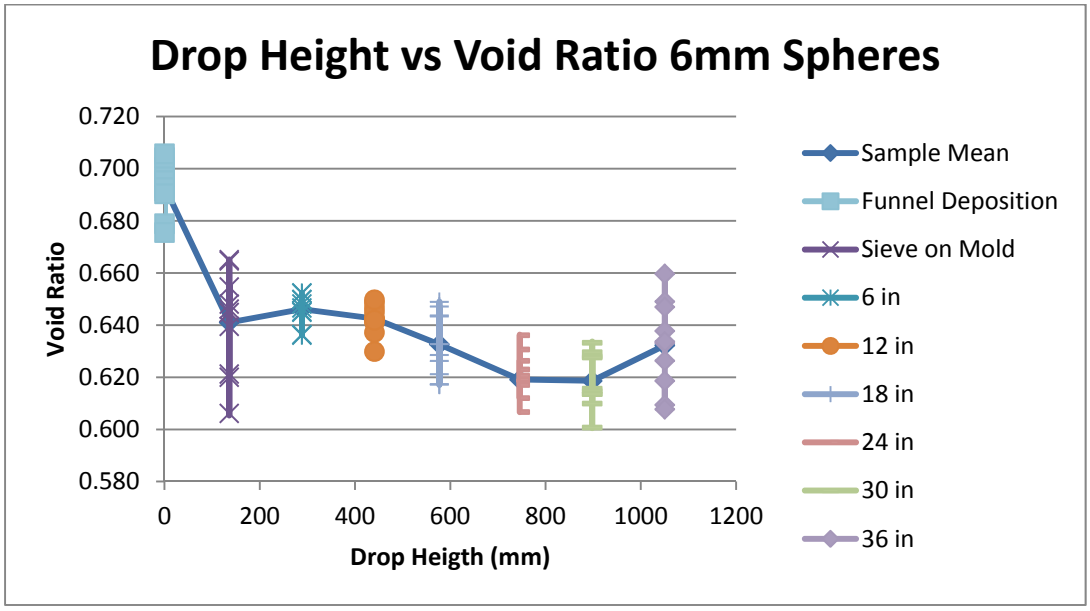

Figure 6: Drop Height vs. Void Ratio for 6mm Sphere Samples

It was assumed that the minimum attainable void ratio was reached when the average weight of the specimen at each drop height stopped increasing. For both the three and six millimeter sphere samples, the minimum attainable void ratio was reached after a drop height of approximately 24 inches. The dispersion of the data at each drop height shows the inherent variability of the experiment, even after securing tight control conditions. Results indicate that, after realizing the standard deviation of the void ratio at each height is fairly uniform, the air pluviation method can be considered as easily repeatable (Table 1).

Table 1: Standard Deviations at Each Sample Height for Specimens Composed of 3 Millimeter Spheres.

Drop Height (mm)	σ Weight	σ Void Ratio
0	0.0093	0.0069
136	0.0124	0.0034
288.4	0.0110	0.0069
440.8	0.0104	0.0063
577	0.0075	0.0067
745.6	0.0102	0.0048
898	0.0039	0.0036
1050.4	0.0134	0.0057

It should be noted that there is more varied dispersion between the sample weights than the measured void ratios. This can be accounted for by recognizing that a lighter sample could still have the same void ratio of a heavier sample, if the light sample has a smaller total volume. For example, samples prepared with three-millimeter spheres at a drop

height of 18 inches have a lower average void ratio as the heavier samples produced at greater drop heights. The lower void ration could only be obtained if the average diameter of the samples prepared at 457 millimeters is lower than the average diameter of samples prepared at the greater drop heights. This variation in total volume can also explain how the average weight of samples decreased from the 30 in drop height to the 36 in drop height, however the void ratio stayed nearly the same for samples prepared using three-millimeter spheres. The higher void ratios for samples prepared using six millimeter spheres occurs on account that the mold size stayed the same but the size of the particles increased. With a larger particle size, larger voids are created throughout the sample.

CHAPTER III

DISCRETE ELEMENT MODEL

3.1 Background

The Discrete Element Method (DEM) was originally conceived by Cundall and Strack in 1979 [1] in order to numerically model granular materials on the micro scale. The program PFC3D, written by ITASCA [21], was used to generate numerical simulations for this research project. The Discrete Element Method uses disks for two-dimensional simulations and spheres for three-dimensional simulations to model individual grains that comprise a granular material. Forces on each particle are determined by applying Newton's Laws of motion at each time step. The numerical algorithm generated by Cundall and Strack also updates the position and possible contacts of particles at each time step [1]. Once particle contacts have been located, the linear contact model was established at the interface between grains. The linear contact model assumes that the contact can be modeled as a spring perpendicular to the grain contact, whose stiffness is determined by input parameters for the normal stiffness of each particle. Friction between particles is taken into account with springs placed parallel to the grain contacts. The shear force is determined from an input parameter for the friction coefficient and shear strength of the particles. A damper is also placed between contacts to account for intrinsic damping inherent to natural phenomena. A graphical representation of grain contact scheme can be seen in Figure 7. Spheres in contact with each other are allowed to overlap to account for the deformation of the

grains. The length of the time step is continually updated to ensure that an adequate amount of calculations can be performed to capture the natural period of the system. This is accomplished by determining the natural frequency of the global system by accumulating the relative stiffness of each contact and the mass of each grain. The time step is then chosen to be one tenth of the period. Since the number of contacts between the particles changes at each time step, the time step for the numerical algorithm is continuously updated.

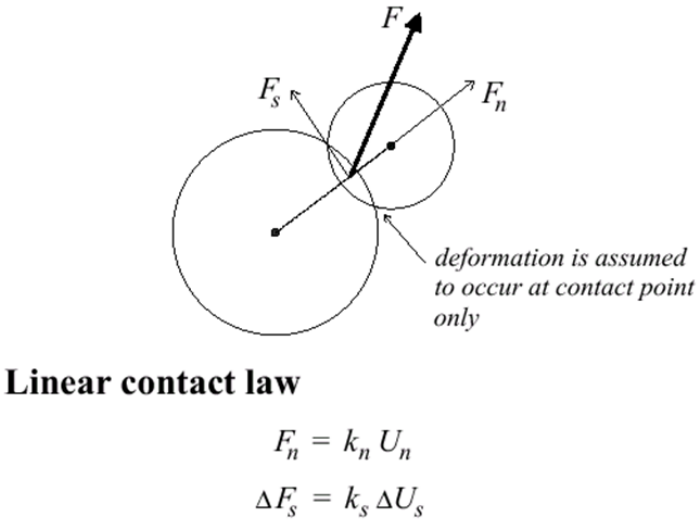

Figure 7: Graphical Representation of the Numerical Scheme for Contacts in the Discrete Element Method [21].

3.2 Model Definition

For the purposes of this research project, a 3D representation of the sample preparation methods described in Chapter 2 were developed. A 2D numerical model was attempted, however the measured porosity of the developed samples could not be

compared to values taken from a three dimensional process due to the difference between planar and global porosity. A sphere size of 6mm was chosen to reduce the computational requirements for each simulation. By modeling 6mm spheres, the total number of particles was reduced from approximately 20,000 to 3,500, and the computational time for each simulation was reduced from over a week to two days. Sphere input parameters such as the normal strength, shear strength, the ball-ball contact friction coefficient, and the ball-wall contact friction coefficient were taken from O'Sullivan and Cui's paper in which Thomson Precision chrome steel spheres were used to calibrate a DEM model for unload reload cycles [20]. The values used for the input parameters can be seen in Table 2. The wall strength parameters were chosen to be much stiffer than the spheres so that the spheres would not be able to penetrate the walls as the simulation was running.

Table 2: DEM Input Parameters

Input Parameter	Value	
Ball Normal Strength	2.02E+11	(Pa)
Ball Shear Strength	7.90E+10	(Pa)
Wall Normal Strength	5.00E+14	(Pa)
Wall Shear Strength	5.00E+14	(Pa)
Ball-Ball Friction	0.096	--
Ball-Wall Friction	0.228	--
Sphere Density	7.83E+03	(kg/m^3)

The split mold, air pluviation tube, and sieve were modeled as cylindrical walls, and the base of the cell was modeled as a disk. The openings for the sieves were modeled by generating intersecting lines to form a mesh that had the same size openings

of 8 mm as the sieve used in the experimental design. The funnel was reproduced numerically by generating a cylindrical wall with a varying radius. 3,500 spheres were then generated above the funnel and allowed to collect in the funnel, dispersed through the sieve, and pluviated through the tube. The porosity of the sample was monitored by calculating the porosity of the sample from three measurement spheres located along the height of the sample. Each measurement sphere had a radius of 33.5 millimeters and was located so that the porosity of the bottom, middle, and top of the sample could be monitored. The simulation was run for twenty million cycles or approximately 48 hours until all of the spheres had settled in the mold.

The funnel deposition numerical model was prepared in the same manner as the air pluviation model, except that the sieves and air pluviation tube were replaced with a smaller diameter tube that extended the throat of the funnel. The tube and funnel were placed so that the bottom of the tube contacted the bottom of the mold. As with the air pluviation model, the spheres were generated above the funnel. The spheres were then allowed to settle under gravity inside the funnel/tube apparatus before an upward velocity of three mm/sec was applied to both the tube and funnel. The simulation was then run for approximately forty million cycles. The porosity of the sample was measured in the same manner as the air pluviation model. Examples of the numerical model layout can be seen in Figure 8 and Figure 9 and the code can be found in Appendix B.

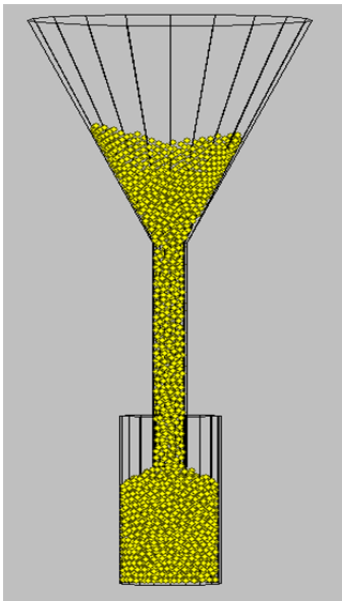

Figure 8: Funnel Deposition Model

Figure 9: Air Pluviation Model

3.3 Results

Due to computational effort, the numerical model was run to simulate the funnel deposition method, and the air pluviation method with drop heights of 136 mm, 577 mm, and 1050 mm. The results from the DEM analysis can be seen in Figure 10. While the numerical model did not follow the mean of the process, some important trends can still be realized from the data. First, it should be noted that the void ratio continues to decrease as the drop height increases. Secondly, all numerical results lie within the range of experimental results as seen in Table 3.

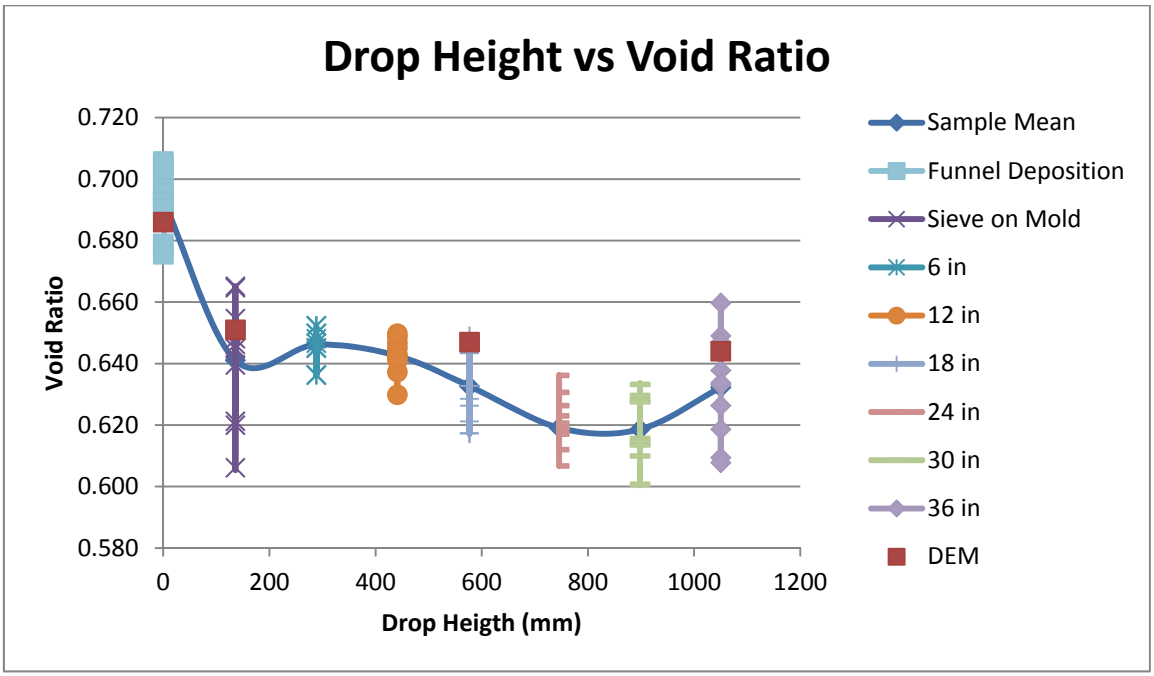

Figure 10: Drop Height vs. Void Ratio Comparing 6mm Sphere Samples with DEM Results

Table 3: DEM and Experimental Void Ratio Results

Drop Height (mm)	DEM Results	Experimental Average	Maximum Void Ratio	Minimum Void Ratio
0	0.686	0.693	0.706	0.676
136	0.651	0.641	0.665	0.606
577	0.647	0.633	0.649	0.617
1050	0.644	0.632	0.649	0.608

Multiple reasons have been postulated to account for the disparity between the numerical model and the true samples. The disparity between results for the funnel deposition method could occur due to an inaccurate measurement of the rate at which the funnel is raised. If the funnel is raised too quickly, the resulting specimen will be more dense. The reverse is true if the funnel is raised to slowly. Since the funnel is raised by hand, a constant rate could not be achieved which could also contribute to the disparity between the results.

Disparity between the results for the air pluviation model could be caused by a difference in the rate at which material flows through the funnel. After recording the sample preparation method of a dense specimen at a drop height of three feet, it was determined that all of the material was deposited in the mold after approximately ten seconds. By multiplying the average time step by the total number of cycles that were necessary to complete the simulation, it was determined that the numerical deposition time is approximately thirty seconds. This disparity could be due to an increase in the amount of friction in the throat of the funnel that restricts the flow of particles and causes an arching affect. The increase in friction could be due to a faulty assumption for the normal and shear strength of the funnel walls, as well as an unrealistic friction

coefficient. The effect of changing these parameters should be investigated to increase the accuracy of the numerical results obtained from the air pluviation simulations.

CHAPTER IV

IMAGE ANALYSIS

In order to characterize the heterogeneity of a typical sample, image analysis techniques were used to gain a perspective on the microstructure of a sample prepared using typical reconstitution methods. This chapter outlines the method used to acquire cross sectional slices of a typical specimen, and the procedures used to segregate the images. After segregation, the variation of void ratio along the height of the sample and within the sample was obtained. Similar procedures were applied to the numerical model to compare the variation of void ratio between the numerical and laboratory experiments.

4.1 Image Acquisition

A dense sample composed of three-millimeter spheres prepared using the air pluviation method at a drop height of three feet was used to characterize the heterogeneity of a typical sample. The Texas A&M Materials Laboratory was used to gather CT scan images of the specimen. Originally vacuum pressure was used to hold the sample in place during the five hour test, however due to the configuration of the CT scanning machine, the split mold was left in place around the sample to contain the specimen during the test procedure and vacuum pressure was not applied. This concession was required since the specimen rotates to obtain a full 360 degree cross sectional slice of the sample. Due to the rotation of the sample, the hose from the vacuum pump could interfere with the CT scanner or distort the sample as it coiled

around the scanning apparatus. The layout of the test procedure can be seen in Figure 11. Slices of the specimen were taken at one-millimeter intervals. A sample image can be seen in Figure 12.

Figure 11: CT Scanner with Prepared Sample in Mold.

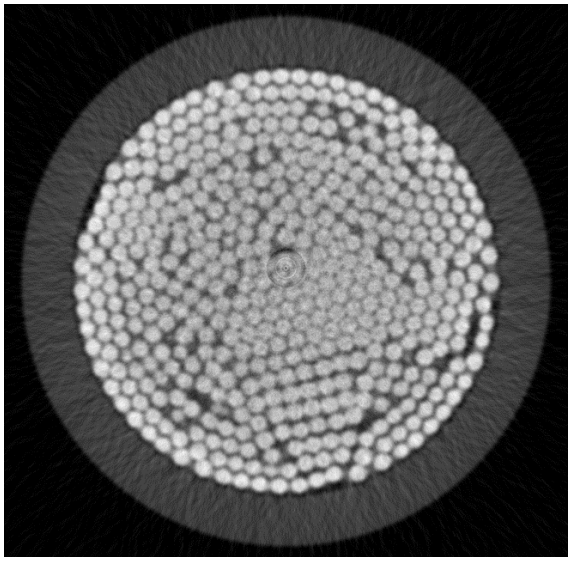

Figure 12: CT Scan Image of a Slice 2mm from the Bottom of a Sample with 3mm Spheres.

4.2 Mold Removal

Since the split mold remained in place during the scan, the mold had to be removed digitally from each slice without deleting portions of the spheres along the mold interior. First the images were cropped using the image analysis program IamgeJ [22]. The image processing toolbox and MATLAB [19] were then used to analyze the images. After loading the image into the MATLAB workspace, a histogram of the image was produced to determine which gray scale were attributed to the mold. A typical histogram can be seen in Figure 13. Based on this histogram, a binary image of only spheres can be generated by thresholding the raw image at a gray scale intensity of 90 to replace all the pixels below the threshold with a zero and all the pixels above with a one. A closing operation was then performed on the binary image to fill in the voids between the spheres. A disk structuring element with a 25 pixel radius was used for this operation. After closing and multiplying the binary image by 255, the inverse of the closed binary image can be subtracted from the original image. The result of this process can be seen in Figure 14.

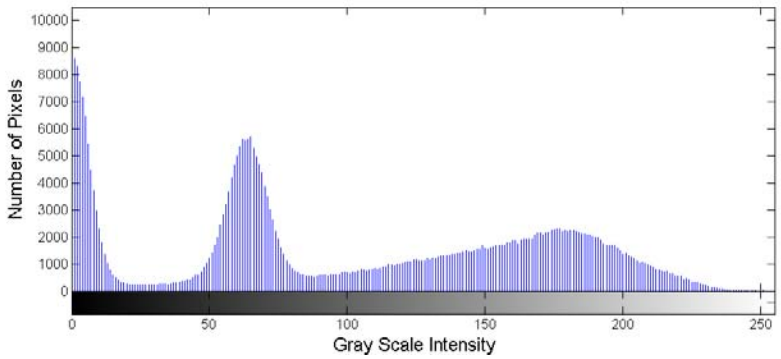

Figure 13: Histogram of the Gray Scale Intensity for a Slice 2mm from the Bottom.

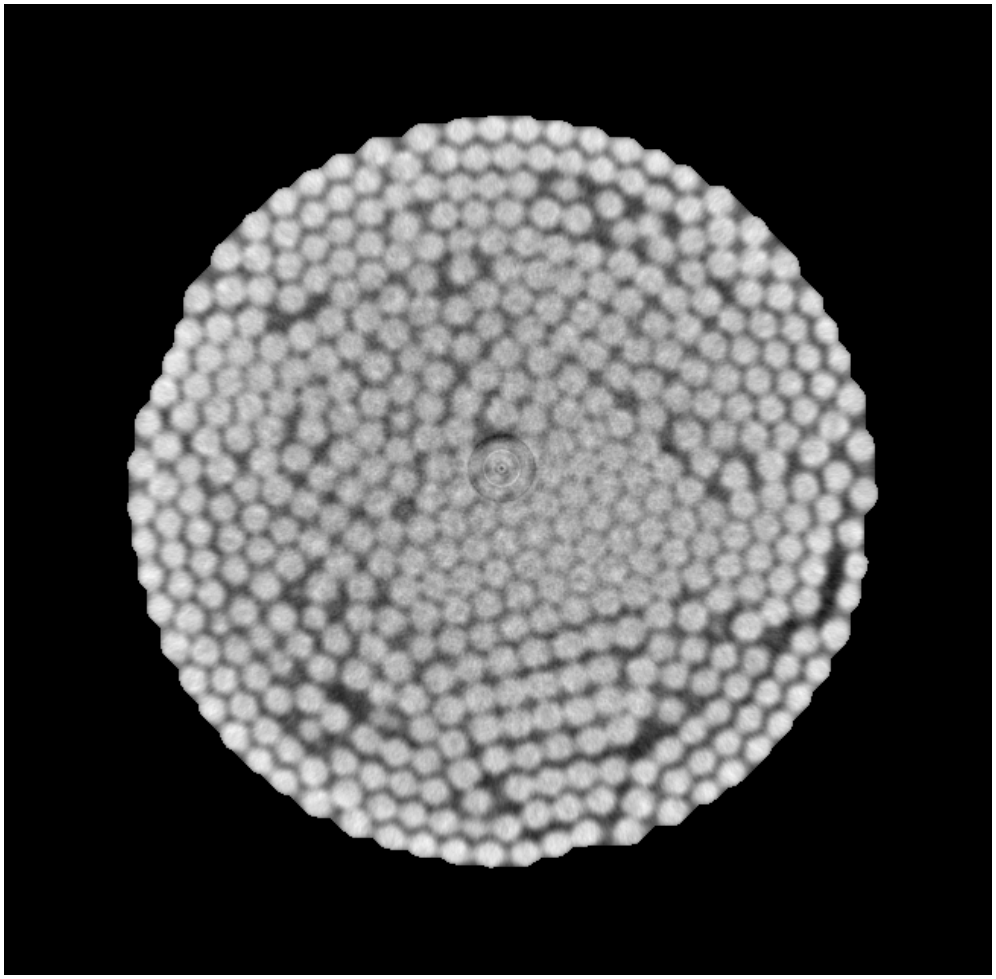

Figure 14: Slice 2mm from the Bottom with No Mold and Intact Interior.

4.3 Isolation of Spheres: Global Threshold Method

After removing all of the extraneous data from the image, the spheres must be isolated in order to accurately calculate the planar void ratio of each slice. To determine a proper threshold level, profiles of the grayscale values of individual spheres were generated. Profiles were taken in both the horizontal and vertical direction through the center of multiple spheres. Sample profiles and their corresponding sphere locations can

be found in Figure 15 through Figure 17. Depending on the location of the sphere within the slice of the mold, a clear threshold value can be determined for the size of the sphere.

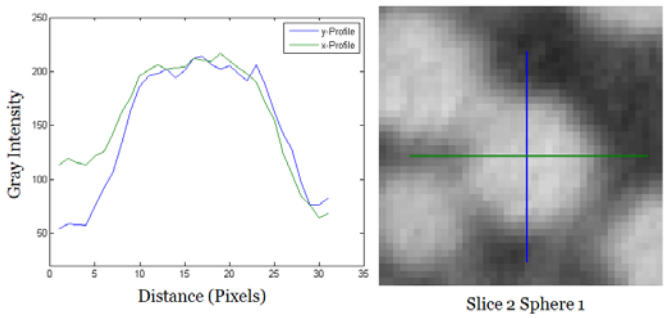

Figure 15: X and Y Sphere Profiles and Locations for Sphere 1, 2mm from the Bottom of the 3mm Sample.

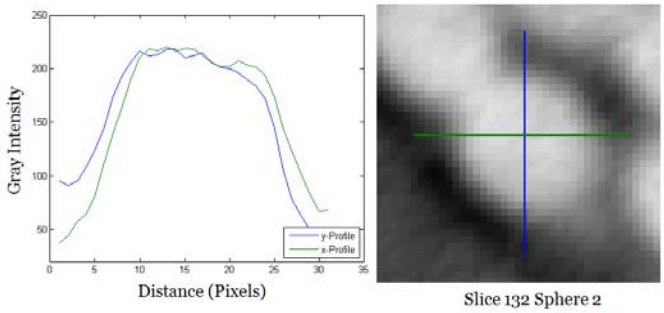

Figure 16: X and Y Sphere Profiles and Locations for Sphere 2, 132mm from the Bottom of the 3mm Sample.

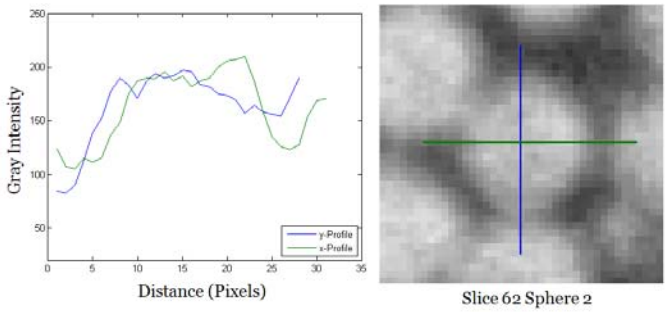

Figure 17: X and Y Sphere Profiles and Locations for Sphere 2, 62 mm from the Bottom of the 3mm Sample.

For example, the sphere profiles for sphere 1 and 2, taken from slice 2 and 132 respectively, show steep peaks in the grayscale intensity around the edges of the sphere. Based on these peeks, a threshold value of 140/255 was used to segment the images. A gray scale value closer to the assumed edge of the sphere was chosen so that as much information about the spheres could be retained after thresholding the images. However as seen in Figure 17, the low threshold value can impede the accuracy of the global method at the contacts between spheres. By looking at the y-profile for sphere 2 taken from slice 62, the threshold level of 140 will not capture the contact. The gray scale values from the interior of the sphere, to the interior of the sphere below, never pass below the threshold level. Sample images using the global threshold method can be seen in Figure 18 and Figure 19.

Depending on the location of the slice along the height of the specimen and the area within the slice, the success of the global threshold method varied. For example, the global method succeeded in segregating the general shape of the spheres, however the contacts between spheres where exaggerated creating large clumps of spheres. This effect can clearly be seen around the edges of the sample and in locations where the spheres are tightly packed together. In some instances, voids located within the tight packs of spheres were completely ignored. Attempts were made to erode the binary image to reduce the contact length, however this process also eroded spheres that were not in contact with others causing an overall reduction in the amount of spheres present in the slice. Another complication with the global method can be seen in Figure 19 in which the spheres cannot be correctly isolated in the interior of the sample. These

complications are greatly exaggerated in images corresponding to locations towards the top of the sample. Due to these complications and a necessity to accurately identify sphere boundaries, new methods were developed to segregate the images.

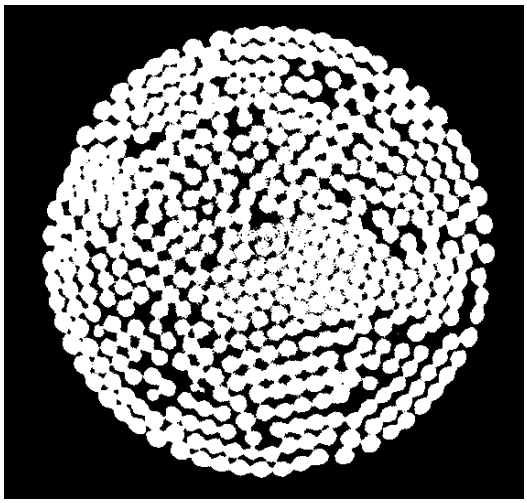

Figure 18: Global Threshold of a Slice 2mm from the Bottom of the 3mm Sphere Sample.

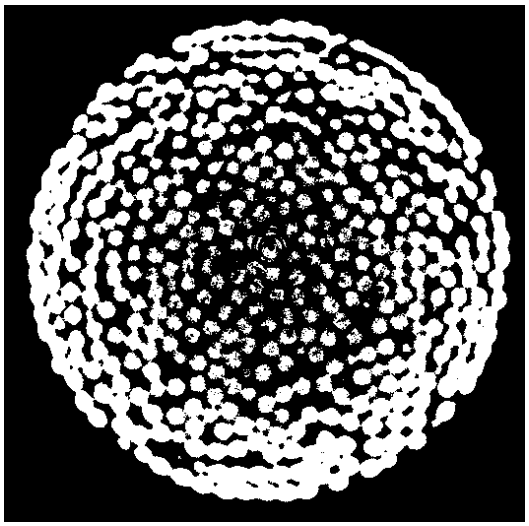

Figure 19: Global Threshold of a Slice 132 mm from the Bottom of the 3mm Sphere Sample.

4.4 Isolation of Spheres: Derivative Method

In order to correctly locate spheres within the center of the specimen, an evaluation of the gray scale values across each slice was made. Profiles were generated in the vertical and horizontal direction through the center of each image. Sample profiles for a slice at the bottom and top of the sample can be seen in Figure 20 and Figure 21. After comparing these profiles, a significant drop in the intensity of the gray scale values in the center of the image can clearly be seen. Because of this decrease, spheres were deleted by the global threshold value used in the previous method. However, even though the profiles in Figure 11 show the decrease in gray intensity, peaks and valleys can still be observed. After recognizing that each profile could be treated as its own signal, the second derivative of each signal could be used to set a new threshold level. Each peak in the signal could be considered as a sphere, while each valley in the signal could be considered a void. By numerically differentiating each signal, the inflection points could be located. Each inflection point would represent the edge of a sphere. Locations at which the second derivative was negative can also be contributed to spheres, since the slope of the signal should always be decreasing and increasing around the center of a sphere. By combining the inflection points with the locations at which the second derivative was negative, spheres could be located with the derivative method.

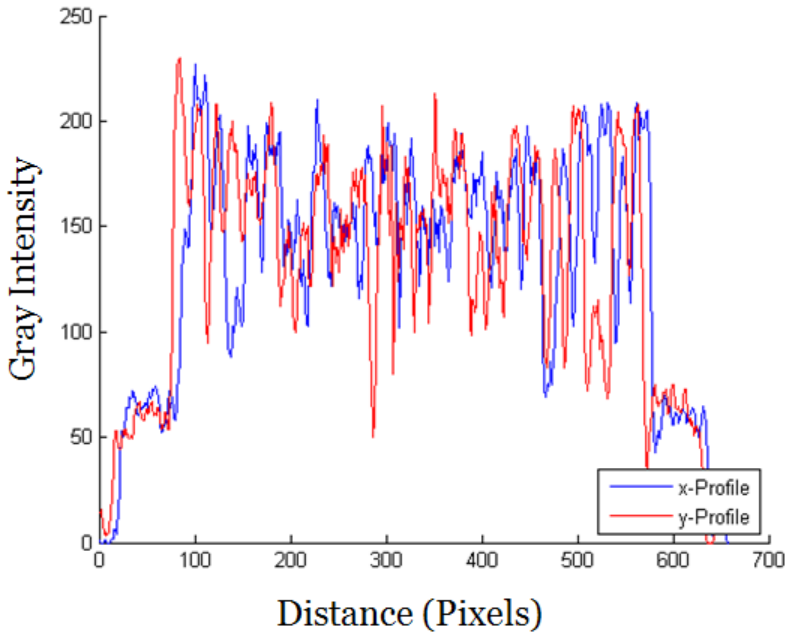

Figure 20: Typical Gray Scale Signals of a Slice 2 mm from the Bottom of the 3mm Sample.

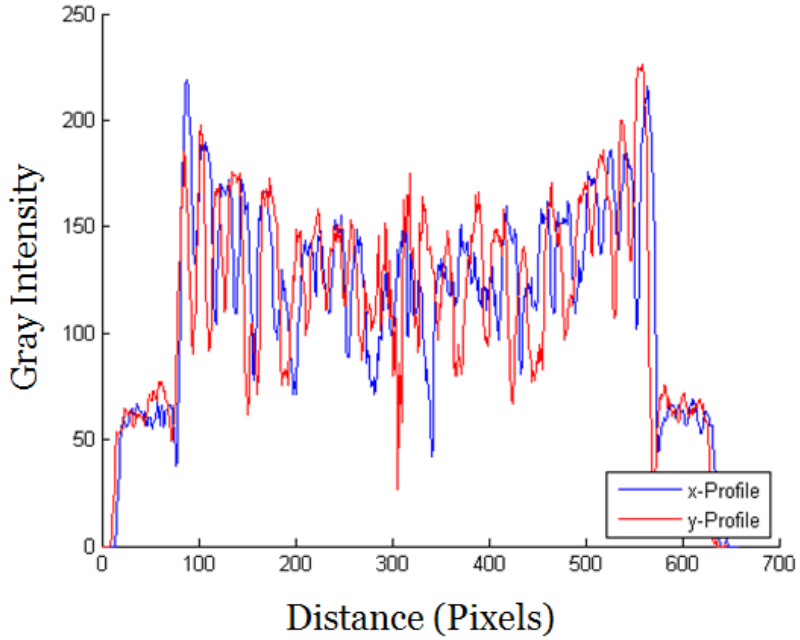

Figure 21: Typical Gray Scale Signals of a Slice 132 mm from the Bottom of the 3mm Sample.

A numerical algorithm was generated with MATLAB [19] to apply the new second derivative threshold method to each slice. A grayscale signal was first compiled from a row of pixels taken from the cropped image. The signal was then smoothed by using the moving average method and the second derivative was calculated numerically using the three point centered method. Multiple window sizes for the moving average method were investigated, and a window size of 11 pixels was chosen. An example of the moving average can be found in Figure 22. Smaller window sizes did not smooth the signal enough to accurately determine the edges of the sphere since the noise within the function would cause the second derivative to be zero at points within the sphere and within the void. Larger window sizes would also inaccurately describe the edges of spheres by removing too much variation in the signal in areas that could be considered the edge of the sphere.

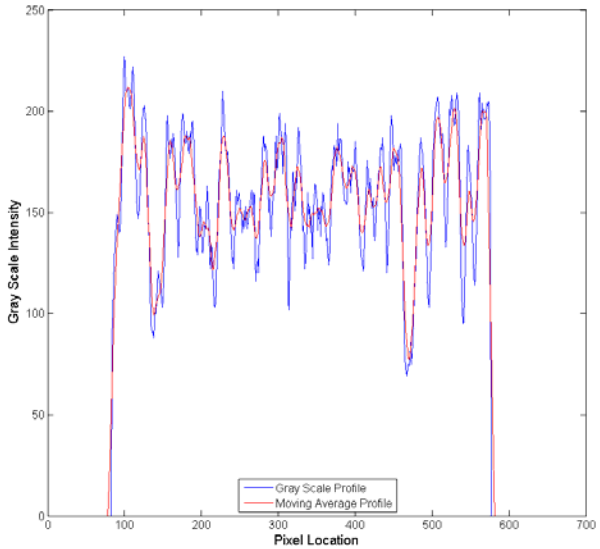

Figure 22: Typical Gray Scale Signal and Calculated Moving Average of a Slice 2mm from the Bottom of the 3mm Sample.

A new image was then created by looping over the points in the second derivative vector. If the value of the second derivative was zero, a one was placed in the new image at the corresponding pixel location. The same occurred if the second derivative was negative. If the second derivative was positive, a zero was placed in the corresponding pixel location within the new image. This method was then repeated by generating a signal from each row and column of pixels in the gray scale image. The two binary images created using this method were able to differentiate the edges of spheres along the direction of the signal. For example, if the image was compiled from signals taken from rows of pixels, voids could be detected on the left and right sides of spheres, but not above or below spheres. This effect can be seen in Figure 23 and Figure 24. In order to completely isolate the spheres, the two images were added together. The final image was assembled by looping over each pixel of the two second derivate compiled images. If the value of the pixels in both images were the same, the corresponding pixel in the final image equaled the value of the pixel in the previous image. For example, if both pixels from the second derivative image equaled one, the corresponding pixel in the final image also equaled one. If the values between the pixels in the two images were different, the corresponding pixel in the final image was set to zero. An example of the final image can be seen in Figure 25. The result of the derivative threshold method produced the opposite effect of enlarging sphere contacts than the traditional threshold method. As can be seen in Figure 15, the spheres located towards the exterior of the sample could easily be separated, while spheres in the center of the sample could not easily be seen. The segregated spheres in the final image also

tend to be angular in appearance. The smooth circular shapes as seen in the global threshold images are hardly seen in the derivative image. Holes also appear in the center of a number of spheres. This could be attributed to small peaks that occur within the larger more pronounced peaks that are considered spheres. Because of these errors in segregating the spheres, another method was conceived.

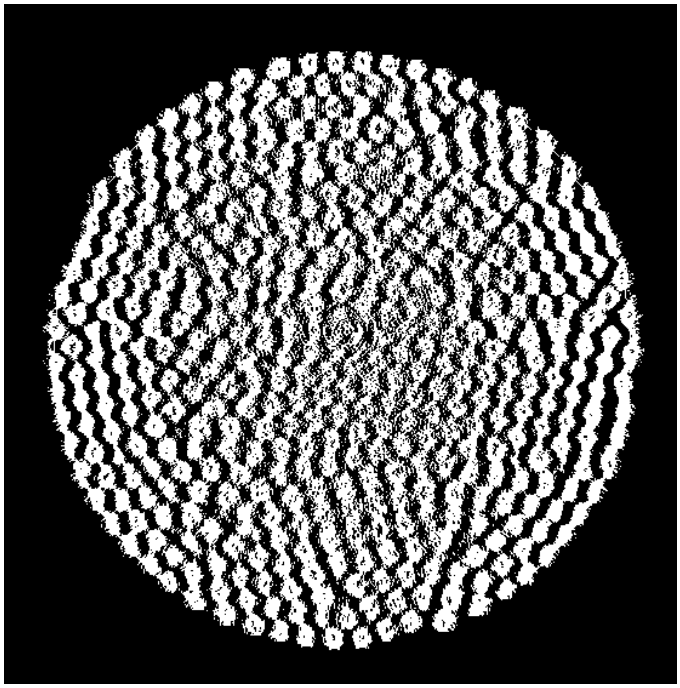

Figure 23: Image Compiled from the Second Derivative of a Signal Compiled from a row of Pixels from a Slice 2mm from the Bottom of the 3mm Sample.

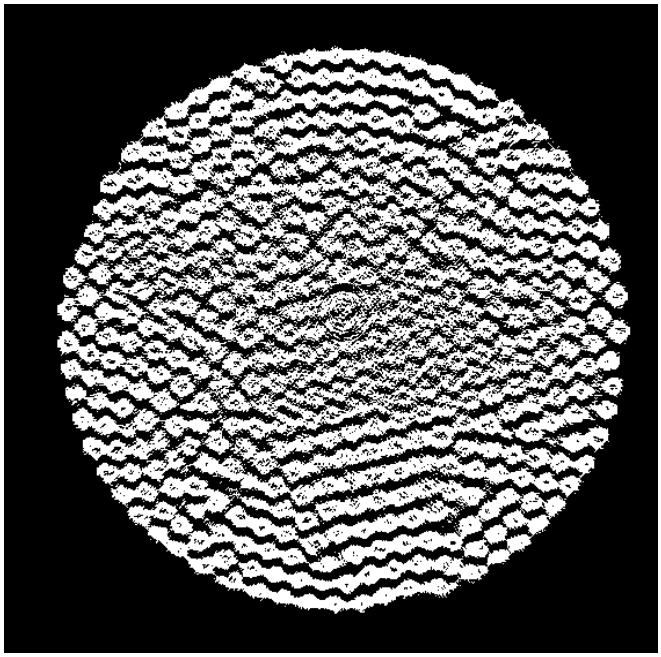

Figure 24: Image Compiled from the Second Derivative of a Signal Compiled from a Column of Pixels from a Slice 2mm from the Bottom of the 3mm Sample.

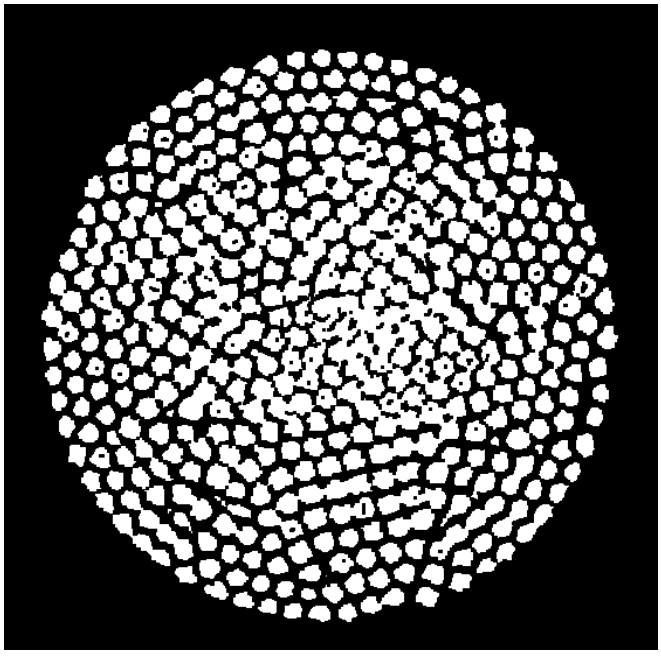

Figure 25: Final Image Reconstruction Using the Derivative Method (Rows + Columns) from a Slice 2mm from the Bottom of the 3mm Sample.

4.5 Isolation of Spheres: Local Threshold Method

In order to separate spheres in both the exterior and interior of the sample and take into account variations in the intensity of the images, a new segregation technique, local thresholding, was considered. By enlarging the window for the moving average, the mean of the process could be approximated while maintaining some of the local variation within each signal. The new smooth signal could then be compared to the original signal compiled from rows or columns of pixel values taken from the gray scale image. In the same manner as the derivative threshold method, two images can be created from different signals and can be combined to form a new binary image.

A numerical algorithm was again generated in MATLAB [19] to perform the local thresholding technique. First a profile was taken from a row or column of gray scale intensities. In order to correctly generate the mean of the process, the moving average of the signal should only be calculated for pixel locations that are located inside of the mold. If this step is ignored, the pixels outside of the sample interior will skew the moving average. For this to be accomplished, the number of points used to calculate the moving average function should be the same as the sum of the row or column from a binary image in which pixels within the interior of the mold have a value of one, while pixels outside of the mold interior have a value of zero. The image required for this purpose was generated while removing the mold as described in the previous section. Since the moving average function only contains as many entries as points located inside the mold, the entries from the moving average function were placed in a new vector of zeros that was the same length as the signal vector. The moving average entries were

placed in the same entries of the vector that corresponded to their original location within the signal. Meaning, if the first value of the moving average function was taken from the 87^{th} pixel in the signal, this value was placed in the 87^{th} entry of the zero vector. An example of a grayscale profile and the corresponding moving average can be seen in Figure 26 A new binary image was then created by assigning a one to any pixel that corresponded to a location at which the signal was greater than the mean of the process. A pixel in the new image was assigned a zero if the signal was less than the mean of the process. The same trend of locating voids in the direction of the signal, as seen in the derivative threshold method, can be observed while comparing images from the local threshold method (See Figure 27 and Figure 28). The two images were then combined in the same manner as the derivative method to create the final image as seen in Figure 29. The final image was dilated to slightly increase the sizes of the spheres by using a square structuring element with a two pixel width. It should be noted that while some exaggerated contacts between spheres are still present, most have been eliminated in the exterior and interior of the sample. This method also accounts for the reduction in grayscale values in the interior of the sample in slices taken from the top of the specimen. This can be seen by comparing Figure 19 and Figure 30. In Figure 19, the interior spheres are almost nonexistent, however the spheres can clearly be identified in the local threshold reconstructed image (Figure 30).

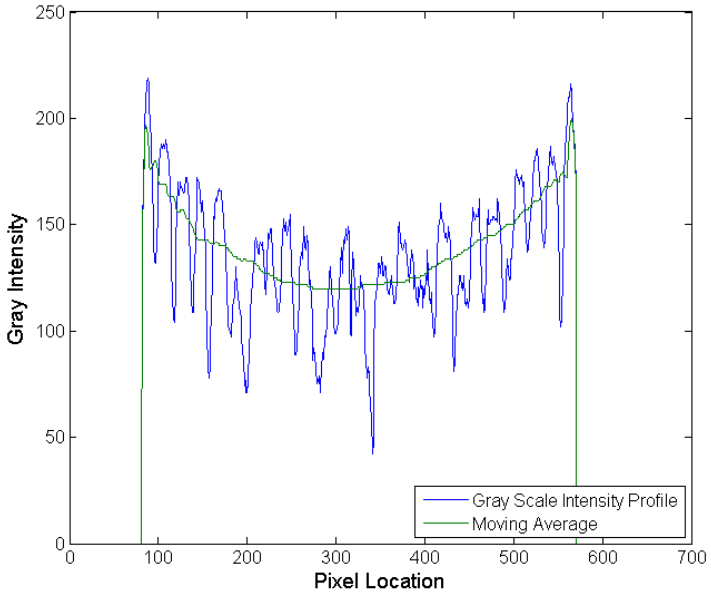

Figure 26: Gray Scale Intensity and Corresponding Moving Average for a Slice Taken 2 mm from the Bottom of the 3mm Sphere Sample.

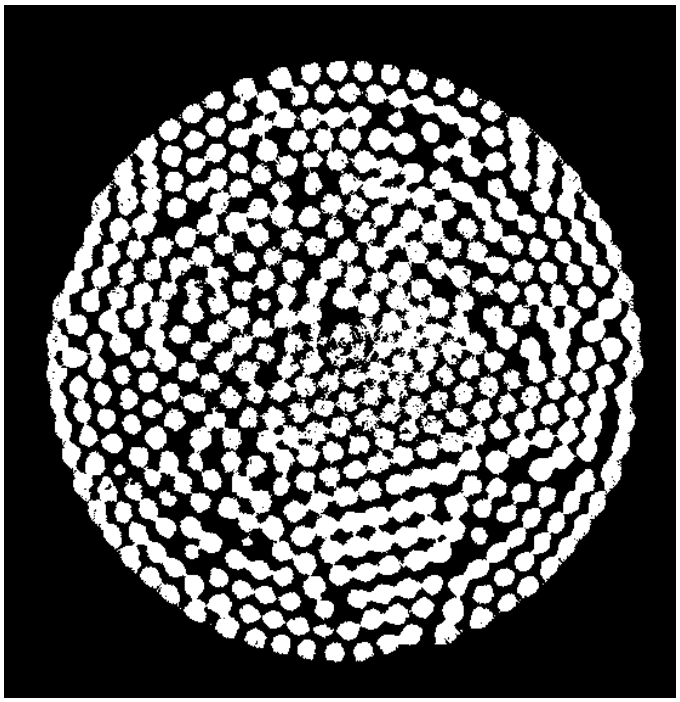

Figure 27: Reconstructed Image from Signals Taken from Rows of Pixels from a Slice 2mm from the Bottom of the 3mm Sample.

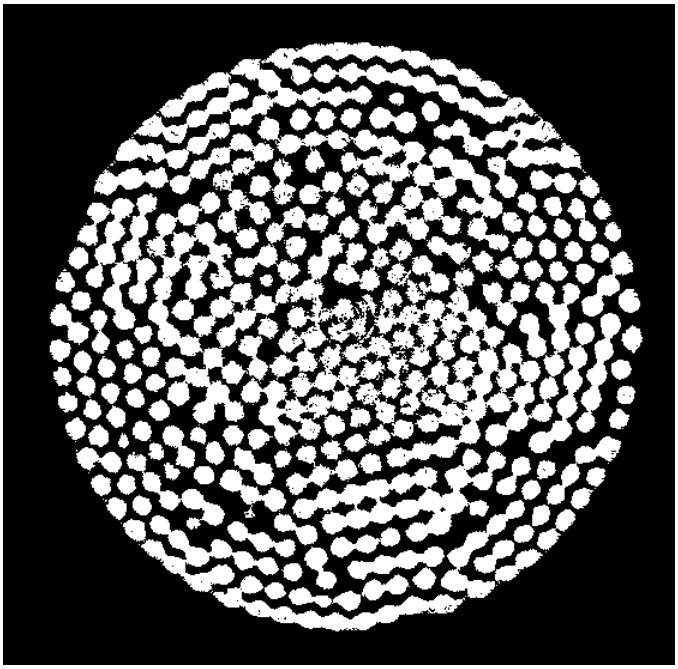

Figure 28: Reconstructed Image from Signals Taken from Columns of Pixels from a Slice 2mm from the Bottom of the 3mm Sample.

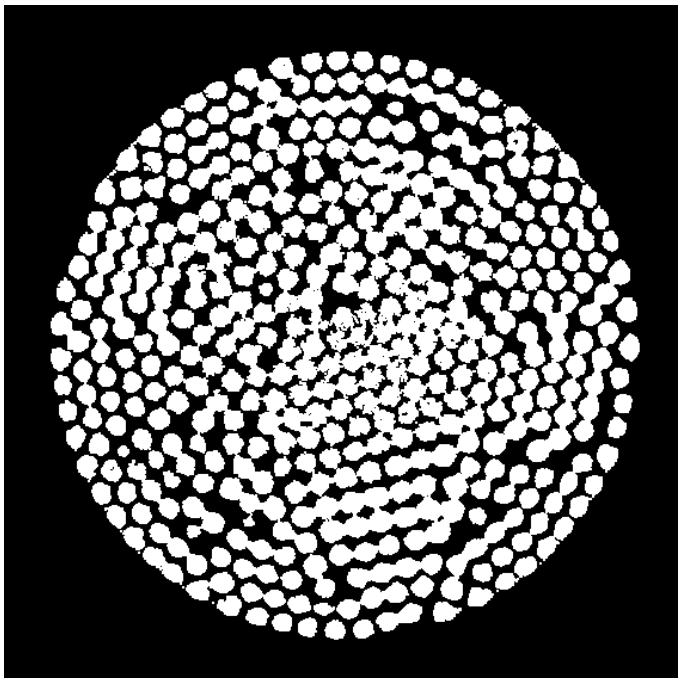

Figure 29: Final Image Using the Local Threshold Method (Rows + Columns) from a Slice 2mm from the Bottom of the 3mm Sample.

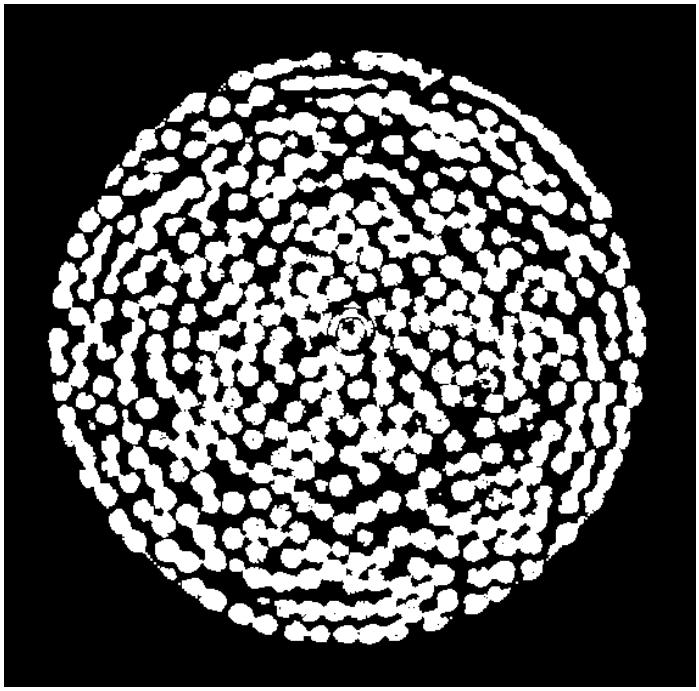

Figure 30: Final Image Using the Local Threshold Method (Rows + Columns) from a Slice 132mm from the Bottom of the 3mm Sample.

4.6 Comparison of Threshold Methods

In order to evaluate which thresholding method was the most accurate, the error between the sphere sizes of the raw image and binary images was calculated. Because of the inaccuracies with the derivative threshold method, as discussed in the previous section, only the traditional method and local method were compared.

Twenty sphere locations were chosen from slice two, and their diameters were recorded using the measure command in the MATLAB [19] image toolbox. Spheres were only taken from the second slice since the range of sphere diameters was known. Knowing that the second slice is located two millimeters above the porous stone and that all spheres located in the second slice are also the lowest spheres in the sample, the

smallest cross sectional radius of a sphere within the slice is approximately 1.4 millimeters. The cross sectional radius was calculated using the Pythagorean Theorem:

$$r = \sqrt{R^2 - z^2}$$

where r is the cross sectional radius, R is the radius of the sphere, and z is the distance between the center of the sphere and the location of the slice. Due to the possibility of the slice being slightly lower than two millimeters from the bottom of the sample, all cross sectional sphere diameters should be within the range of 3 to 1.4 millimeters. The ratio between pixels and millimeters was determined by measuring the distance between the interior edges of the mold. The interior mold diameter was measured to be exactly 72 millimeters with the use of digital calipers. With this known distance, each millimeter was determined to be seven pixels in both the X and Y directions. Therefore the range of sphere diameters should be within 21 to 10 pixels. The results of the comparisons between methods can be seen in Table 4. A comparison of sphere diameters as highlighted in the table can be seen in Figure 31.

After inspecting the data, the global threshold method tends to exaggerate the sizes of the spheres, while the local threshold method tends to reduce the area of the spheres. A positive error corresponds to the threshold method producing larger spheres than the raw image, while negative values refer to spheres being smaller than the raw image. The large discrepancies between sphere diameters occurred in areas where spheres were closely packed together. Due to the exaggeration of the contacts within the global threshold method, the global method on average created spheres that were 5% larger than the raw image. Since the spheres were more isolated within the local

Table 4: Comparison of Sphere Diameters and Threshold Methods.

Sphere Diameters (Pixels)			Percent Error	
Raw Image	Global Image	Local Image	Raw vs Global	Raw vs Local
21	20	18	-5%	-14%
19	21	20	11%	5%
17	17	16	0%	-6%
18	18	18	0%	0%
16	17	17	6%	6%
19	20	19	5%	0%
18	18	17	0%	-6%
19	20	19	5%	0%
18	20	19	11%	6%
20	20	19	0%	-5%
18	18	16	0%	-11%
18	19	18	6%	0%
17	18	16	6%	-6%
16	18	17	13%	6%
17	19	18	12%	6%
20	23	19	15%	-5%
16	15	15	-6%	-6%
17	19	17	12%	0%
16	18	16	13%	0%
18	19	19	6%	6%
		Average:	5%	-1%

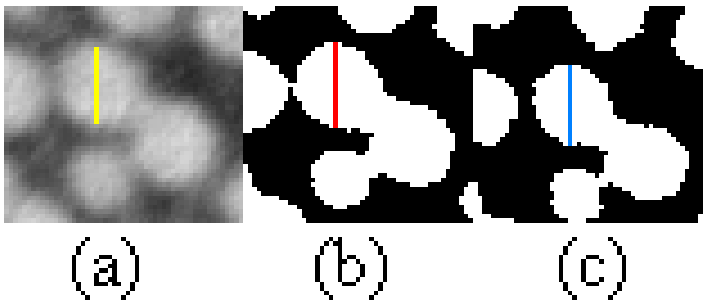

Figure 31: Comparison of Sphere Diameters from the Raw Image (a), the Global Image (b), and the Local Image (c). Diameter Lengths are Highlighted in Table 4.

method, the error between sphere diameters was reduced to 1%. Based on this comparison, the local threshold method was used to further analyze the void ratio of the samples.

4.7 DEM Image Reconstruction

In order to compute the void ratio of the numerical models, a method was developed to create cross sectional slices of the numerical sample. In order to reconstruct the images, the position of the centroid of each sphere was exported into Excel. The table was then imported into MATLAB [19]. Sphere with centroids located above 133 millimeters from the bottom were deleted from the centroid vector since these excess spheres would be removed from the mold by the ruler. A vector of slice heights was then created ranging from 1 to 135 in one millimeter intervals. While looping over each slice height, the distance between the center of the sphere above the base of the sample and the height of the slice was calculated. Since the spheres are circular, the size of the cross section of the sphere would be the same if the slice is above or below the sphere centroid. The distance between the centroid and the slice height was only calculated if the center of the sphere was within three millimeters of the slice. The radius of the cross section of the sphere was then calculated using the Pythagorean Theorem as described in the previous section. The location of the centroid within the slice was determined by using the x and y position taken from the numerical model. A typical slice of the numerical sample prepared at a three-foot drop height can be seen in Figure 32.

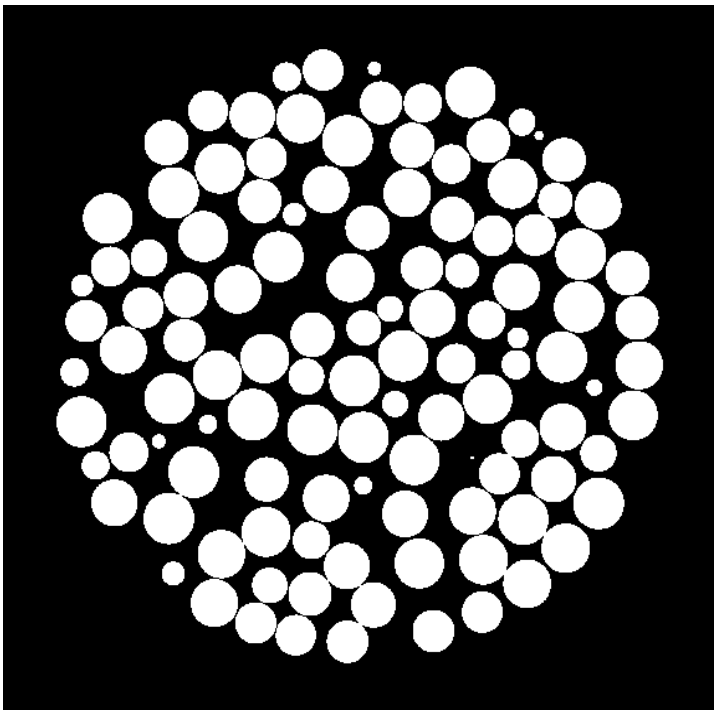

Figure 32: Slice 66 from a Numerical Sample with 6mm Spheres.

4.8 Planar Void Ratio Variation

The first metric used to determine if modeling the sample preparation techniques could capture the spatial heterogeneity and microstructure of the sample was the planar void ratio. The planar void ratio was computed for each image captured along the height of the sample and for each slice generated from the numerical model as described in the previous section. The planar void ratio was calculated by first creating a binary image of each slice. The local threshold method was used to create the binary images from the CT scan results. Since the matrix describing a binary image is only composed of ones and zeros, the summation of all the values in the binary image matrix equals the total area of spheres within the slice. The total area within the mold was calculated with the

known inner diameter of the mold of 72 mm and the ratio of 7 pixels per millimeter. The void ratio was then calculated by dividing the quantity of total area minus the area of spheres divided by the area of spheres. Results from the planar void ratio analysis can be seen in Figure 33 and Figure 34.

While a direct comparison cannot be made between the results, due to the fact that the sample used in the CT scan analysis was composed of three-millimeter spheres while the numerical model is composed of six-millimeter spheres, some important trends can be realized. First, the distribution of the void ratio varies greatly at the bottom of each sample. This can be explained by the tight packing of spheres that occurs at the sample base. For example, the void ratio will be significantly lower at a slice intersecting the center of the spheres when all of the spheres are at the same elevation. This naturally occurs at the bottom of the sample. As we move up the height of the sample, the variation of the void ratio decreases significantly. As the packing of the particles becomes more random, the cross sectional area of the spheres becomes more varied and the void ratio becomes more uniform. A second similarity between the two methods can be seen as the void ratio dramatically increases at the top of the sample. This increase in the void ratio occurs due to the removal of particles at the top of the sample. The increase also occurs since there are no longer any spheres to fill the voids created by the spheres below. The slight decrease at approximately 15 millimeters from the top of the three-millimeter sample could be due to the reduction in the drop height as material is placed in the mold. The difference between the experimental and planar void ratios is due to the volumetric affect. If the full volumetric integral is computed, the

experimental void ratio and the void ratio computed from the image analysis should converge.

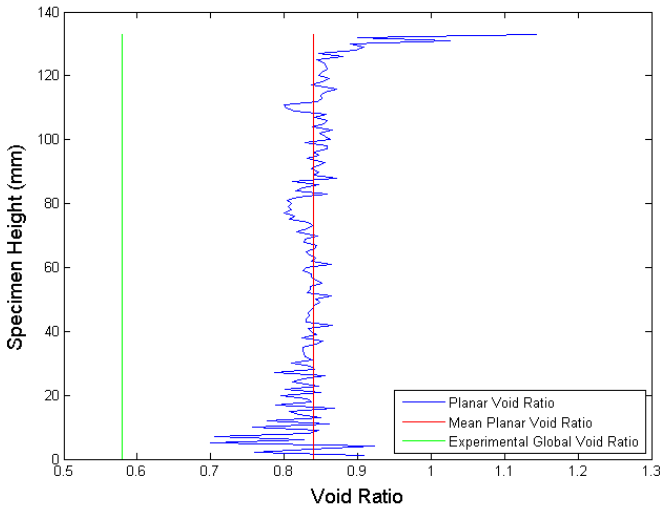

Figure 33: CT Scan Planar Void Ratio along the Height of the 3mm Sphere Sample

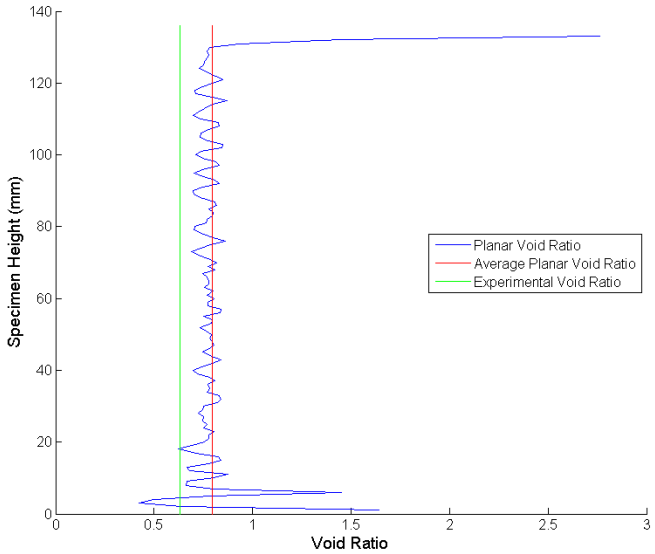

Figure 34: Numerical Model Planar Void Ratio along the Height of a 6mm Sphere Sample.

4.9 Void Ratio Variation within Each Slice

The second metric used to quantify the spatial heterogeneity of each specimen was to quantify the variation of the void ratio within each slice. The variability of the void ratio was determined by examining the void ratio at multiple control points with varying control areas. The control point locations were determined by defining a mesh grid with a spacing of 10 pixels between each control point. A grid was selected to assess the void ratio to ensure a uniform distribution of points throughout the sample. The location of the control points can be seen in Figure 35. The void ratio was calculated over square control areas ranging from 5 to 110 pixels. In order to reduce the error of the void ratio calculated at control points located near the edge of the specimen, the size of the control area was also limited to remain within the mold interior. The control area was also used to define the total area while calculating the void ratio at each point. To allow the total area to change, the total area was calculated as the sum of pixels located within the control area from a binary image where all pixels in the mold interior had a value of one and pixels outside of the mold were zero. The distribution of the size of the control area when the maximum width is 110 pixels can be seen in Figure 36. The area of spheres was determined by computing the sum of the control area from the binary image computed using the local threshold method. As expected, the mean of the void ratio converges to an estimated value as the control area increased. The variability of the void ratio between the control points also decreased as the control areas increased. These two trends can be seen in Figure 37 and Figure 38. Contour plots of the void ratio variation for the 3 mm sphere sample can be seen in Figure 39 through

Figure 41. All contour plots shown were constructed using a control area of 110 by 110 pixels.

As can be seen, the void ratio varies throughout the cross section of the slice. As seen in Figure 39, there is a dense collection of spheres near the center of the sample and a region with a high void ratio below and to the left of the center of the sample. These areas can clearly be seen in both the contour plot and the raw image. The same patterns of high heterogeneity at the bottom of the sample and lower heterogeneity above, as seen in the As the packing of the spheres becomes more random, the sample tends to become more homogeneous, however different regions within the slice range from a void ratio of approximately 0.85 to 0.6. For a specimen to be truly homogeneous, the void ratio should be nearly constant throughout the sample.

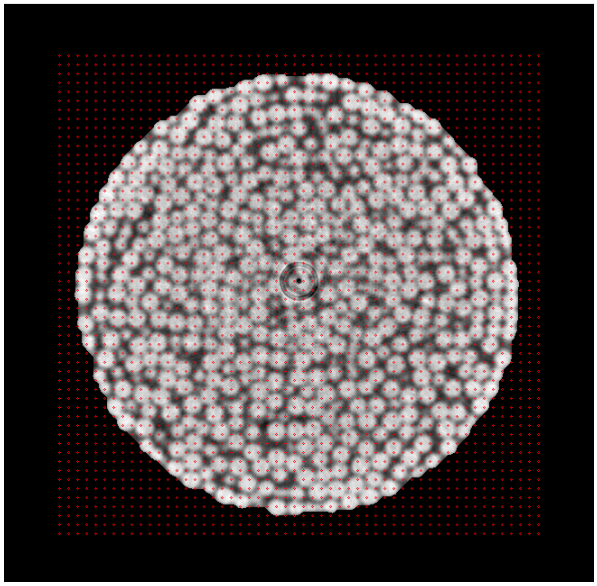

Figure 35: Locations of the Control Points are Shown in Red.

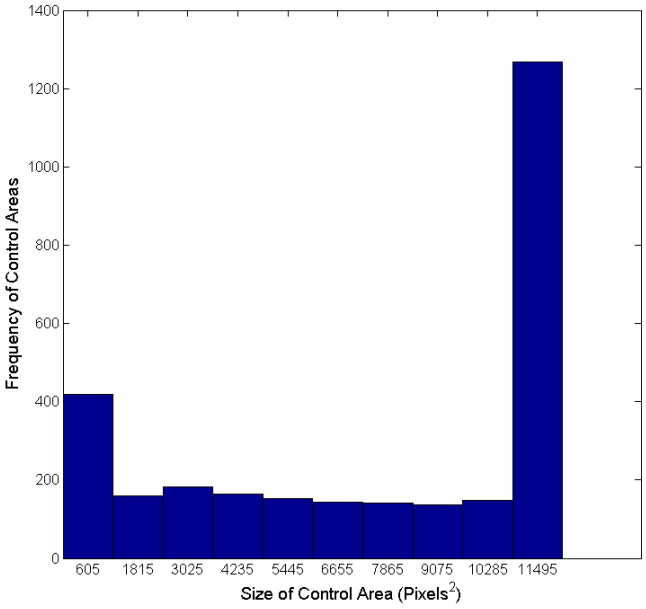

Figure 36: Size Distribution of Control Areas when the max Control Area is 110x110 Pixels. The Distribution of Points Occurs so that the Control Area only Includes Points Within the Mold.

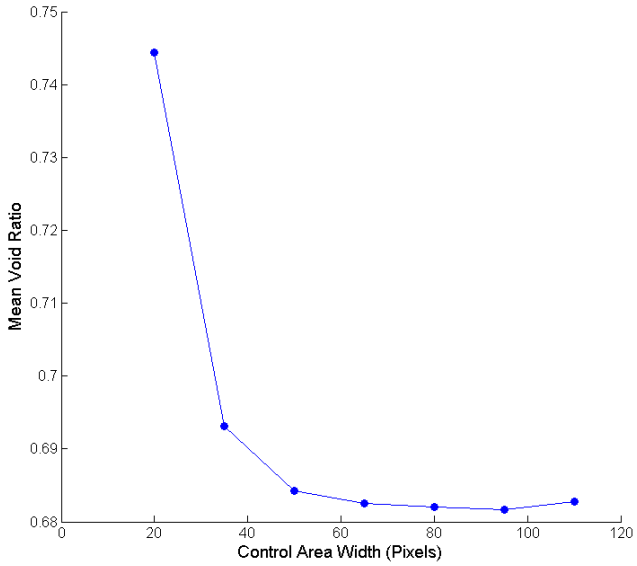

Figure 37: Mean Void Ratio for all Control Points vs. the Size of the Control Area for a Slice 2 mm from the Bottom of the 3mm Sphere Sample.

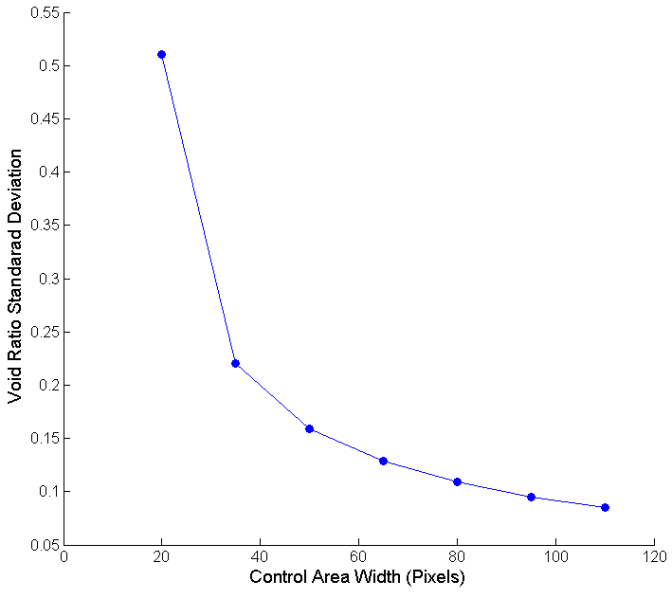

Figure 38: The Standard Deviation of the Void Ratio for all Control Points vs. the Size of the Control Area for Slice 2 mm from the Bottom of the 3mm Sphere Sample.

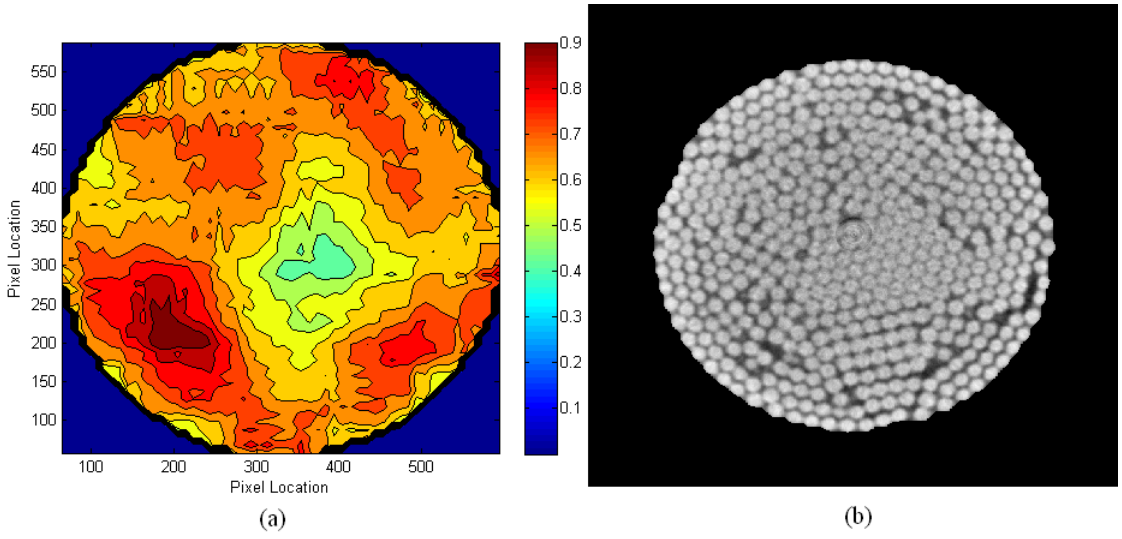

Figure 39: Void Ratio Contour Plot with 110x110 Control Areas (a) of a Slice 2mm from the Bottom of the 3mm Sphere Sample (b).

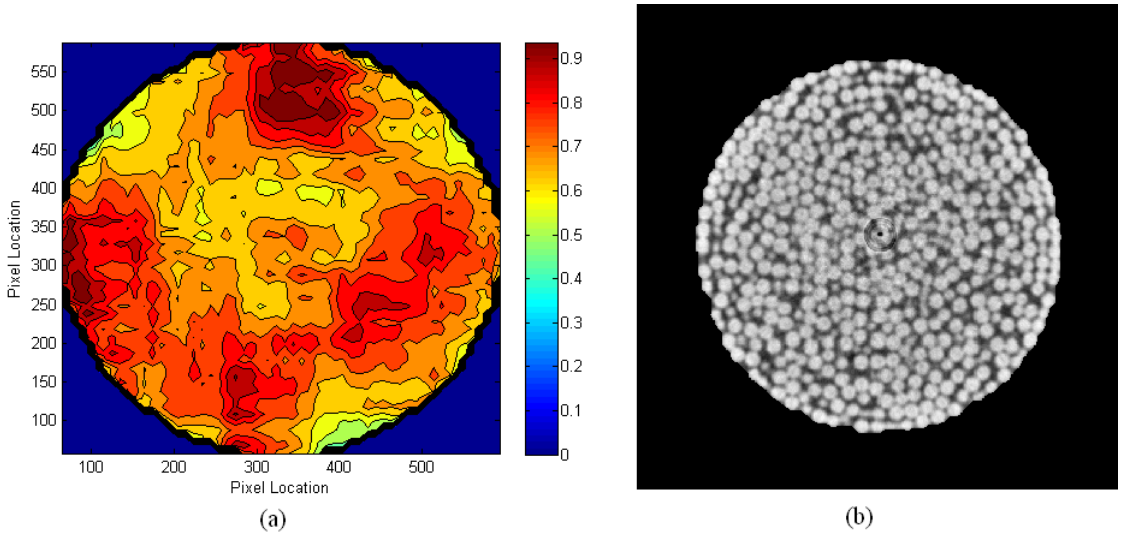

Figure 40: Void Ratio Contour Plot with 110x110 Control Areas (a) of a Slice 66mm from the Bottom of the 3mm Sphere Sample (b).

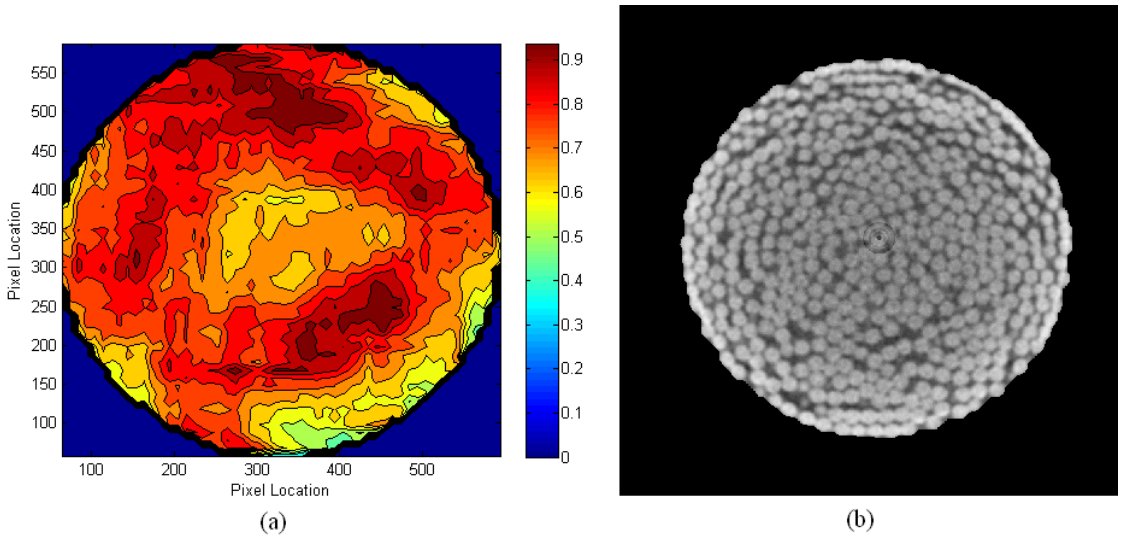

Figure 41: Void Ratio Contour Plot with 110x110 Control Area (a) of a Slice 132mm from the Bottom of the 3mm Sphere Sample (b).

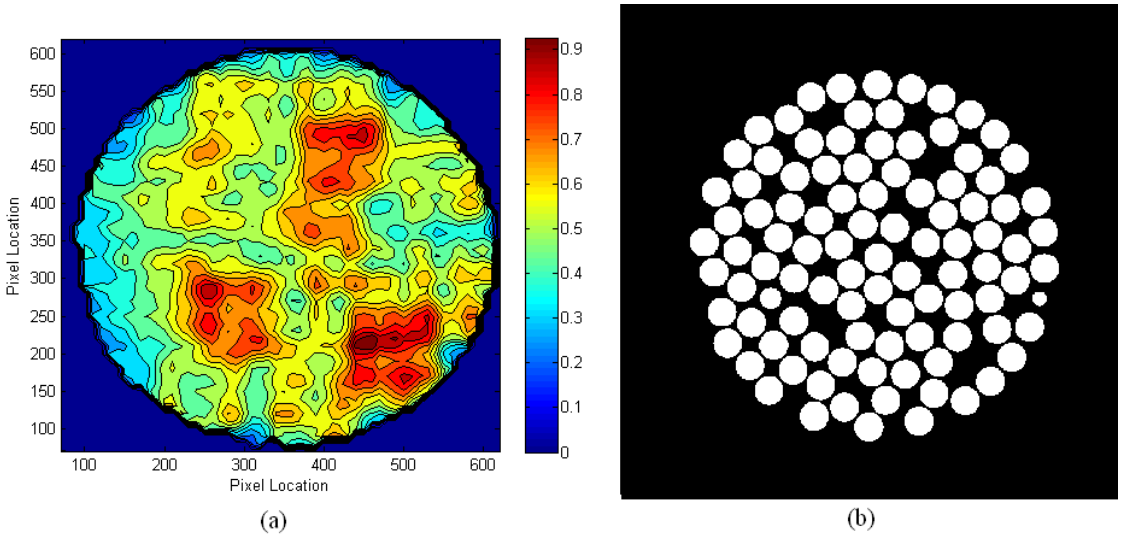

Figure 42: Void Ratio Contour Plot of a Numerical Sample with 110x110 Control Areas (a) of a Slice 2mm from the Bottom of the 6mm Sphere Sample (b).

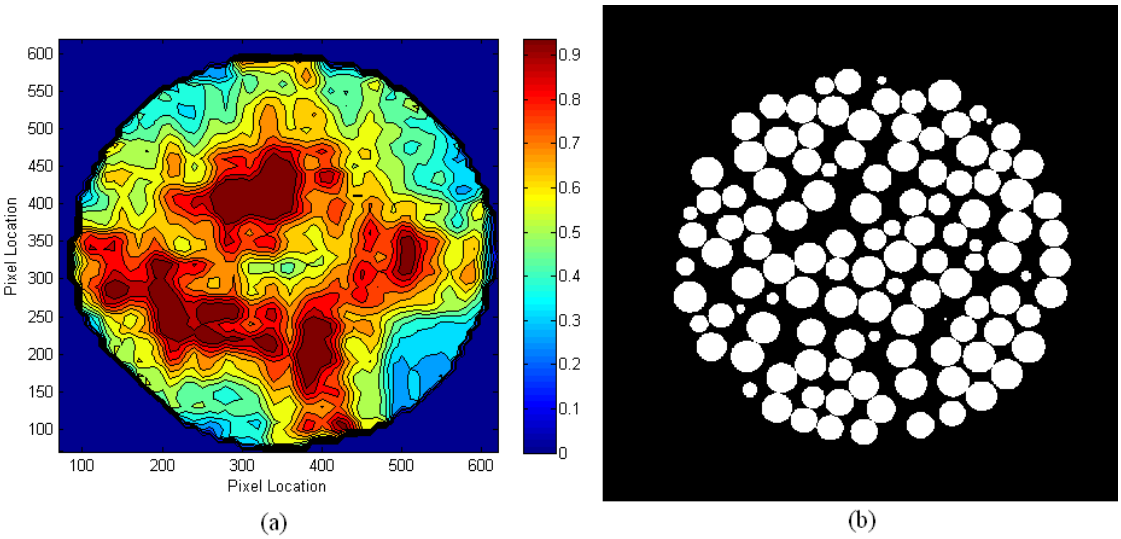

Figure 43: Void Ratio Contour Plot of a Numerical Sample with 110x110 Control Areas (a) of a Slice 66mm from the Bottom of the 6mm Sphere Sample (b).

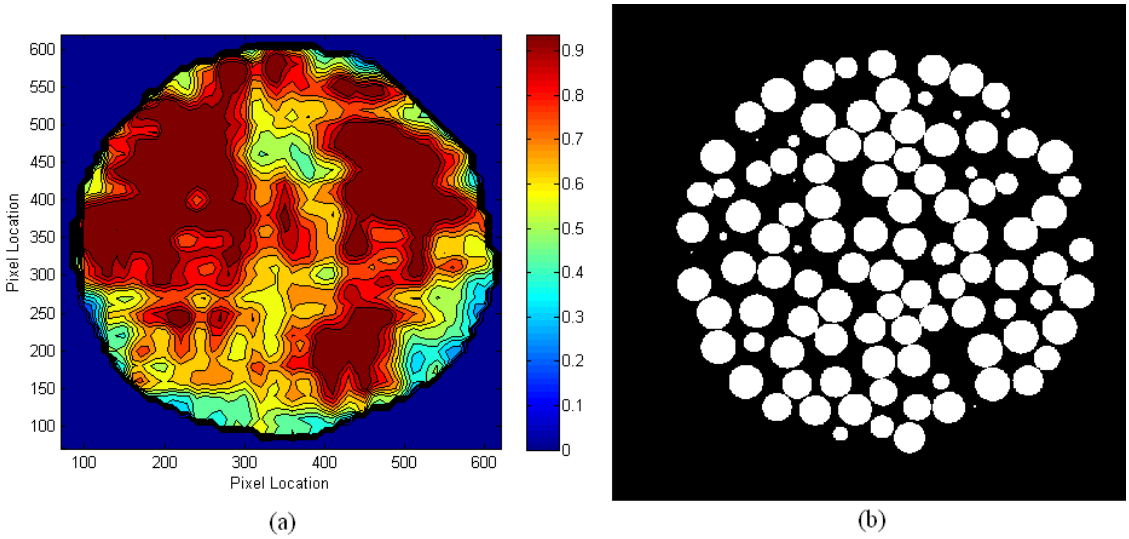

Figure 44: Void Ratio Contour Plot of a Numerical Sample with 110x110 Control Areas (a) of a Slice 131mm from the Bottom of the 6mm Sphere Sample (b).

Contour plots showing the spatial distribution of the void ratio with slices of a numerical sample can be seen in Figure 42 through Figure 44. As with the sample prepared in the lab, the void ratio varies greatly within each slice. The bottom slice also contains the largest areas of dense compactions of spheres, while the void ratio becomes more evenly distributed at higher sample heights. As the packing between particles becomes more random, the voids are more evenly distributed throughout the slice in both the numerical and experimental results. However, areas of higher density are still present in the exterior regions of the slice. These regions most likely occur due to the spheres flowing against the sides of the mold as the sample is formed. The reproduced numerical slices also show much larger voids when compared to the sample composed with three millimeter spheres. These larger voids contribute to the higher void ratios observed while preparing samples with the six millimeter spheres in the laboratory.

Since the results of modeling the sample preparation technique numerically agrees with the trends seen with the three millimeter sample, it can be assumed that the numerical model correctly captures the heterogeneity caused by the sample preparation method.

CHAPTER V

TRIAXIAL COMPRESSION TESTS

In order to compare the effect of the microstructure of the granular material on the global behavior of the sample, a comparison can be made between numerical and experimental results for a triaxial compression test. Multiple experiments were conducted on samples prepared using the funnel deposition method and three millimeter spheres. An isotopic confining pressure of 80 kPa was applied to the sample by use of the vacuum pump. Results from two experiments with samples reconstituted with 3 mm spheres can be found in Figure 45. Even with a high confining pressure, the stress strain response for these samples indicates a loose specimen, as there is no post peak behavior present. An example of a dense sample reconstituted using the air pluviation method at a 3 foot drop height and 40 kPa of confining pressure can be seen in Figure 46. It should be noted that even though the 6 mm specimen was denser than the 3 mm sample, the peak stresses are nearly identical (68 kPa and 70 kPa respectively). Even though the 6 mm sphere sample is denser than the 3 mm sphere sample, it still behaves as a loose specimen. This behavior could be attributed to the lower confining stress and larger voids present within the 6mm sample. It is worth mentioning that it would be beneficial to conduct numerical experiments on both the homogeneous and heterogeneous numerical samples to assess the effect of the microstructure on the global behavior of the specimen.

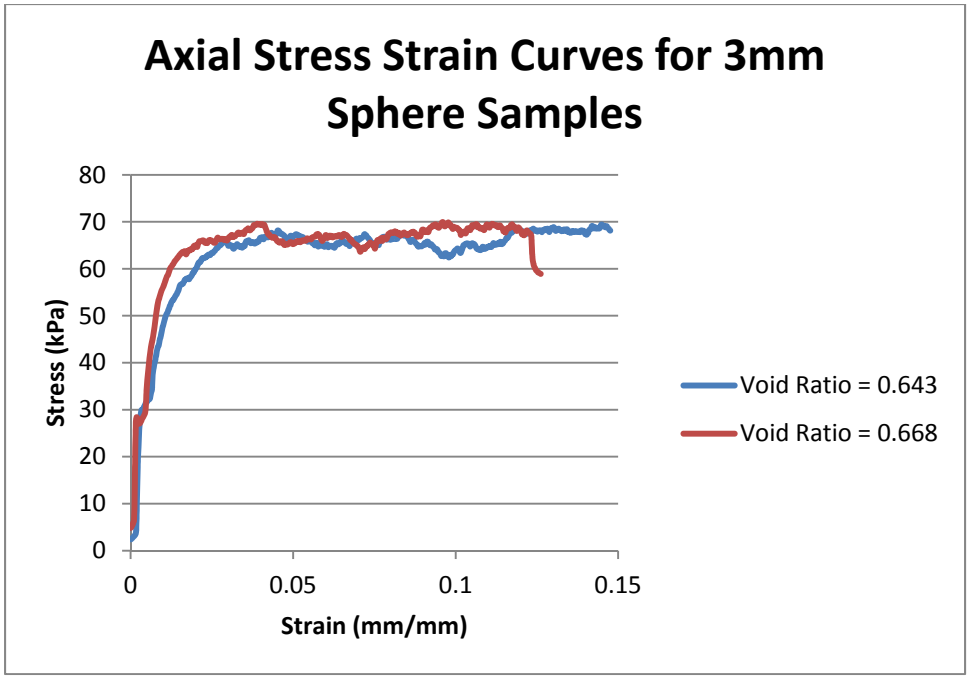

Figure 45: Stress Strain Response for a Loose 3mm Sphere Sample.

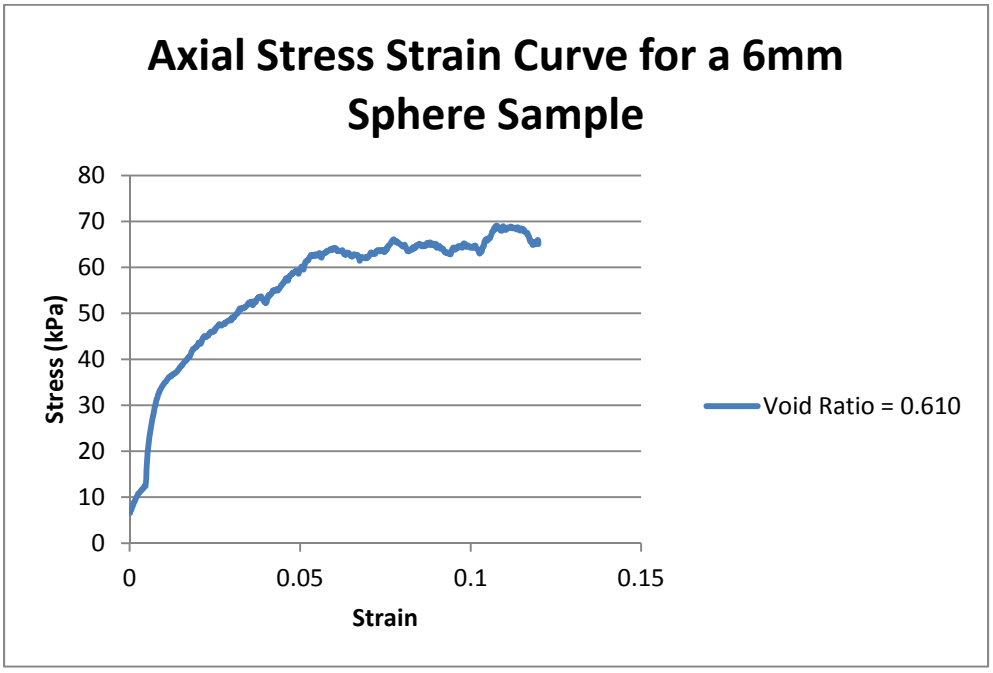

Figure 46: Stress Strain Response for a Dense 6mm Sphere Sample.

CHAPTER VI

CONCLUSION

6.1 Summary

In order to capture the heterogeneity of reconstituted granular materials, two common sample preparation techniques were used to generate specimens of various densities. The air pluviation method was used to produce dense samples, while the funnel deposition method was used to create loose specimens. In order to determine the spatial variability of the samples, x-ray computed tomography was used to capture the internal structure of a dense specimen. The local threshold method was developed to segregate the particles that allowed for a variation in the grayscale intensities of the images and segregation of the spheres in both the interior and exterior regions of the sample. The local method improved the segregation of the images when compared to the global method by reducing the errors associated with the contacts of the grains, so that only 1% error remained between the size of the spheres in the binary image and raw image.

The sample preparation techniques were modeled numerically using the Discrete Element Method. While the numerical results did not match the mean of the void ratio of comparable samples produced in a controlled environment, the numerical models did match the trend of increasing the sample density as the drop height increased. Increased friction in the throat of the funnel could have caused arching between the grains in the numerical model, which could decrease the void ratio of the resulting sample.

The spatial variability of both a numerical and experimental sample was investigated. While a direct comparison could not be made between the two cases due to a difference in grain sizes, certain trends in the variability of the samples were observed. In both the numerical and experimental sample, the variability of the void ratio was higher at the bottom of the sample than at the top. This variation was attributed to the more organized packing of the particles towards the bottom of the sample. As the packing became more random, the variation in the void ratio decreased. This trend not only occurred throughout the height of the sample, but within each slice at different elevations. The slices towards the bottom of the sample had a larger variation of the void ratio due to regions of tightly packed particles and large voids. As the packing of particles became more random, the voids were more evenly distributed throughout each slice and areas of higher density decreased. Areas of higher density tended to be located in the exterior regions of the sample, which most likely occurred due to particles flowing towards the sides of the mold during the preparation of the sample. Since the numerical results follow the trends observed from the experimental results, modeling of the sample preparation techniques can be used to accurately describe the heterogeneity of reconstituted granular materials.

6.2 Future Research

A more detailed analysis of the improvement in the heterogeneity of samples should be researched further by comparing the results of a triaxial test performed on the granular material described in the work. By modeling the sample preparation techniques, a heterogeneous sample can be created that matches the general spatial

distribution of particles of an experimental sample reconstituted in the laboratory. The benefits of this numerical preparation technique can be determined by numerically performing a triaxial test on a homogeneous sample and on a heterogeneous sample. A multiphysics approach can also be analyzed by introducing pore pressure to the sample and coupling the numerical experiment with a finite element program such as FLAC to introduce pore pressure into the Discrete Element Model.

The effect of grain size distribution on the heterogeneity of samples should also be investigated. If smaller grains are present, the distribution of voids will change due to the fact that the smaller grains will fill the voids generated by the larger particles. This can be investigated by preparing samples using the sample preparation techniques described, and a combination of the six and three millimeter steel ball bearings.

More accurate images should also be obtained in order that the spatial distribution of the void ratio can be extended to three dimensions. If the images are more clear and accurately capture the contact between grains, the spheres should be able to be completely segregated from each other. It would then become possible to reconstruct an accurate three dimensional virtual sample by locating the centroids of all the particles in the sample and to measure the spatial variability in three dimensions.

Furthermore, it would also be beneficial to construct a mathematical representation of the spatial variability of the specimen. This heterogeneous mathematical model could then be easily implemented in a Discrete Element Model or be used in multiple applications such as investigations on the propagation of damage through materials.

REFERENCES

[1] Cundall PA, Strack OD L. A Discrete Numerical Model for Granular Assemblies. Geotechnique 1979; 29: 47-65.

[2] Tao H, Jin B, Zhong W, Wang X, Ren B, Zhang Y, and Xiao R. Discrete Element Method Modeling of Non-Spherical Granular Flow in Rectangular Hopper. Chemical Eningeering and Processing 2010; 49: 151-58.

[3] Lu M, McDowell GR. Discrete Element Modeling of Railway Ballast Under Monotonic and Cyclic Triaxial Loading. Geotechnique 2010; 60: 459-67.

[4] Wu J, Collop AC, McDowell GR. Discrete Element Modeling of Constant Strain Rate Compression Tests on Idealized Asphalt Mixture. Journal of Materials in Civil Engineering 2011; 23(1): 2-11.

[5] Potyondy DO, Cundall PA. A Bonded-Particle Model for Rock. International Journal of Rock Mechanics & Mining Sciences 2004; 41: 1329-364.

[6] Garboczi EJ Three-Dimensional Mathematical Analysis of Particle Shape Using X-ray Tomography and Spherical Harmonics: Application to Aggregates Used in Concrete. Cement and Concrete Research 2002; 32: 1621-638.

[7] Grigoriu M, Garboczi E, Kafali C. Spherical Harmonic-Based Random Fields for Aggregates Used in Concrete. Powder Technology 2006; 166: 123-38.

[8] Johnson SM. Resolution of Grain Scale Interactions Using the Discret Element Method. [M.S. Thesis]. Cambridge (MA): Massachusetts Institute of Technology; 2006.

[9] Latham JP, Munjiza A, Garcia X, Xiang J, Guises R. Three-dimensional Particle Shape Acquisition and Use of Shape Library for DEM and FEM/DEM Simulation. Mineral Engineering 2008; 21: 797-805.

[10] Liu XE, Garboczi E, Grigoriu M, Lu Y, Erdogan S. Spherical Harmonic-Based Random Fields Based on Real Particle 3D Data: Improved Numerical Algorithm and Quantitative Comparison to Real Particles. Powder Technology 2010; 207: 78-86.

[11] Mahmoud E, Gates L, Massad E, Edrogan S, Garboczi E. Comprehensive Evaluation of AIMS Texture, Angularity, and Dimension Measurments. Journal of Materials in Civil Engineering 2010; 22: 369-79.

[12] Di Renzo A, Cello F, DiMaio FP. Simulation of the Layer Inversion Phenomenon in Binary Liquid-Dluidized Beds by DEM-CFD with a Drag Law for Polydisperse Systems. Chemical Engineering Science 2011; 66(13): 2945-958.

[13] Viad YP, Sivathayalan S, Stedman D. Influence of Specimen-Reconstituting Method on the Undrained Response of Sand. Geotechnical Testing Journal 1999; 22(3): 187-95.

[14] Yammamuro JA, Wood FM, Lade PV. Effect of Depositional Method on the Microstructure of Silty Sand. Canadian Geotechnical Journal 2008; 45: 1538-555.

[15] Thomson PR, Wong RCK. Specimen Nonuniformities in Water-Pluviated and Moist-Tamped Sands Under Undrained Triaxial Compression and Extension. Canadian Geotechnical Journal 2008; 45(7): 939-56.

[16] Monkul MM. Influence of Silt Size and Content on Static Liquefaction Potential of Sand [Dissertation]. Corvallis (OR): Oregon State University; 2010.

[17] Jiang MJ, Konrad JM, Leroueil S. An Efficient Technique for Generating Homogeneous Specimens for DEM Studies. Computers and Geotechnics 2003; 30: 579-97.

[18] Fu X, Dutt M, Bentham AC, Hancock BC, Cameron RE, and Elliott JA. Investigation of Particle Packing in Model Pharmaceutical Powders Using X-Ray Microtomography and Discrete Element Method. Powder Technology 2006; 167: 134-40.

[19] MathWorks. MATLAB - The Language of Technical Computing [Computer Program on Disk]. Version 7.6.0. Natick (MA): 2012.

[20] O'Sullivan C, Cui L. Micromechanics of Granular Material Response During Load Reversals: Combined DEM and Experimental Study. Powder Technology 2009; 193: 289-302.

[21] Itasca Consulting Group. PFC3D (Particle Flow Code in Three-Dimensions) [Computer Program on Disk]. Version 3.10. Minneapolis (MN): 2005.

[22] Rasband W. ImgaeJ [Computer Program on Disk]. Version 1.45. Bethesda (MD): National Institute of Mental Health; 2012.

APPENDIX A

Figure 47: As can be Seen, the Split Mold is Held in Place with two Hoop Clamps. One at the Base of the Mold, One towards the Top. The Membrane is also in Place and Being Held Against the Sides of the Mold by the Vacuum Pump.

Figure 48: Mold and Triaxial Cell with Air Pluviation Tube in Place.

Figure 49: Material Flowing through the Mold while the Sieve Disperses the Material across the Area of the Tube.

Figure 50: Removing Excess Material with a Steel Ruler.

Figure 51: Weight of Remaining Material.

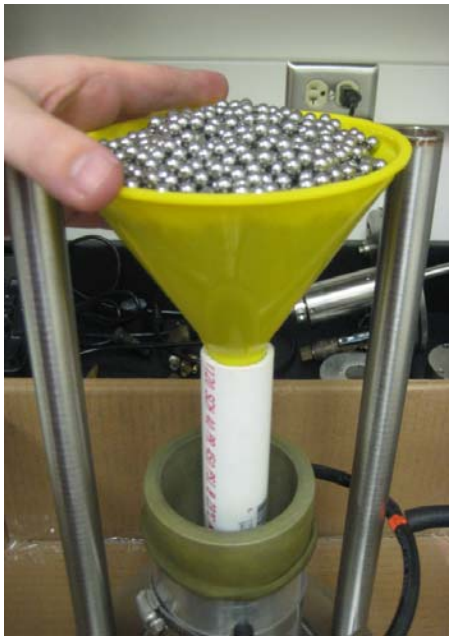

Figure 52: Funnel Deposition Apparatus.

Figure 53: Material Slowly Being Deposited in the Mold.

Figure 54: Final Sample Composed of 6 mm Spheres.

Figure 55: Final Sample Composed of 3 mm Spheres.

APPENDIX B

```
new
set log on
set logfile 3ftballposition
;.....................................................................
;Filename:  airpluv_6mm.dvr
;Author: Patrick Noble
;This Program generates a sample with use of the air pluviation method and 6mm spheres.
;Note units are in mm-kg-sec
;.....................................................................

set gravity 0 0 -9810

;.....................................................................
;Parameters FISH Function
;.....................................................................
define params
        _knwall = 500000000 ;wall normal stiffness
        _kswall = 500000000
        _knball = 202240  ;ball normall stiffness
        _ksball = 79000
        _wfric = 0.228 ;wall friction coefficient
        _bfric = 0.096 ;ball-ball friction coefficient
        _moldh = 150 ;mold height
        _moldr = 35.5 ;mold radius
        _platenr = _moldr + 3 ;base radius
        _tubelength = 3 ;tube length in feet
        _tubeh = _tubelength*12*25.4 ;tube length in mm
        _tuber = 35.5 ;tube radius
        _tubestart = _moldh
        _tubeend = _tubestart + _tubeh
        _sieveh = 101.6 ;sieve hieght
        _siever = 35.5 ;sieve radius
        _sievestart = _tubeend
        _sieveend = _sievestart + _sieveh
        _losh = _sieveend - 30
        _sosh = _sieveend - 66
        _funnelstart1 = _moldh + _tubeh + _sieveh + 4
        _funnelh1 = 20 ;funnel mouth height
        _funnelh2 = 200 ;funnel hieght
        _funnelend1 = _funnelstart1 + _funnelh1
        _funnelstart2 = _funnelend1
        _funnelend2 = _funnelstart2 + _funnelh2
        _funnelr1 = 10 ;mouth radius
        _funnelr2 = 100 ;bowl radius
        _br = 3 ;ball radius
        _bv = (4*3.14159*(_br)^3)/3 ;ball volume
        _mv = _moldh*3.14159*(_moldr)^2 ;mold volume
        _targetporosity = 0.4
        _nb = _mv*_targetporosity/_bv ;number of balls to achieve desired porosity
        _nbg = _nb + 2000 ;number of balls to generate
        _balldens = 0.000007832 ;ball  density
        _genh1 = _funnelend2
        _genh2 = genh1 + 500
        _genb1 = _funnelr2*0.7
        _genb2 = -1*_genb1
end
```

```
params


;.....................................................................
;Generate walls for sample containment
;.....................................................................
wall type cylinder end1 0 0 0 end2 0 0 _moldh rad _moldr _moldr kn _knwall ks _kswall f _wfric
wall type disk rad _platenr norm 0 0 1 kn _knwall ks _kswall f _wfric

;.....................................................................
;Generate walls for pluviation tube
;.....................................................................
wall type cylinder end1 0 0 _tubestart end2 0 0 _tubeend rad _tuber _tuber kn _knwall ks _kswall f _wfric

;.....................................................................
;Generte Funnel
;.....................................................................
wall type cylinder end1 0 0 _funnelstart1 end2 0 0 _funnelend1 rad _funnelr1 _funnelr1 kn _knwall ks _kswall f
_wfric
wall type cylinder end1 0 0 _funnelstart2 end2 0 0 _funnelend2 rad _funnelr1 _funnelr2 kn _knwall ks _kswall f
_wfric
wall origin 0 0 _funnelstart1 norm 0 0 1 kn _knwall ks _kswall f _wfric id 1000

;.....................................................................
;Generate lines for sieves
;.....................................................................
wall type cylinder end1 0 0 _sievestart end2 0 0 _sieveend rad _siever _siever kn _knwall ks _kswall f _wfric
;LARGE OPENING SIEVE
wall type line3d end1 -4 35.5 _losh end2 -4 -35.5 _losh kn _knwall ks _kswall f _wfric
wall type line3d end1 -16 35.5 _losh end2 -16 -35.5 _losh kn _knwall ks _kswall f _wfric
wall type line3d end1 -24 35.5 _losh end2 -24 -35.5 _losh kn _knwall ks _kswall f _wfric
wall type line3d end1 -32 35.5 _losh end2 -32 -35.5 _losh kn _knwall ks _kswall f _wfric
wall type line3d end1 4 35.5 _losh end2 4 -35.5 _losh kn _knwall ks _kswall f _wfric
wall type line3d end1 16 35.5 _losh end2 16 -35.5 _losh kn _knwall ks _kswall f _wfric
wall type line3d end1 24 35.5 _losh end2 24 -35.5 _losh kn _knwall ks _kswall f _wfric
wall type line3d end1 32 35.5 _losh end2 32 -35.5 _losh kn _knwall ks _kswall f _wfric
wall type line3d end1 35.5 -4 _losh end2 -35.5 -4 _losh kn _knwall ks _kswall f _wfric
wall type line3d end1 35.5 -16 _losh end2 -35.5 -16 _losh kn _knwall ks _kswall f _wfric
wall type line3d end1 35.5 -24 _losh end2 -35.5 -24 _losh kn _knwall ks _kswall f _wfric
wall type line3d end1 35.5 -32 _losh end2 -35.5 -32 _losh kn _knwall ks _kswall f _wfric
wall type line3d end1 35.5 4 _losh end2 -35.5 4 _losh kn _knwall ks _kswall f _wfric
wall type line3d end1 35.5 16 _losh end2 -35.5 16 _losh kn _knwall ks _kswall f _wfric
wall type line3d end1 35.5 24 _losh end2 -35.5 24 _losh kn _knwall ks _kswall f _wfric
wall type line3d end1 35.5 32 _losh end2 -35.5 32 _losh kn _knwall ks _kswall f _wfric
;SMALL OPENING SIEVE
;wall type line3d end1 0 35.5 _sosh end2 0 -35.5 _sosh kn _knwall ks _kswall f _wfric
;wall type line3d end1 5 35.5 _sosh end2 5 -35.5 _sosh kn _knwall ks _kswall f _wfric
;wall type line3d end1 10 35.5 _sosh end2 10 -35.5 _sosh kn _knwall ks _kswall f _wfric
;wall type line3d end1 15 35.5 _sosh end2 15 -35.5 _sosh kn _knwall ks _kswall f _wfric
;wall type line3d end1 20 35.5 _sosh end2 20 -35.5 _sosh kn _knwall ks _kswall f _wfric
;wall type line3d end1 25 35.5 _sosh end2 25 -35.5 _sosh kn _knwall ks _kswall f _wfric
;wall type line3d end1 30 35.5 _sosh end2 30 -35.5 _sosh kn _knwall ks _kswall f _wfric
;wall type line3d end1 35 35.5 _sosh end2 35 -35.5 _sosh kn _knwall ks _kswall f _wfric
;wall type line3d end1 -5 35.5 _sosh end2 -5 -35.5 _sosh kn _knwall ks _kswall f _wfric
;wall type line3d end1 -10 35.5 _sosh end2 -10 -35.5 _sosh kn _knwall ks _kswall f _wfric
;wall type line3d end1 -15 35.5 _sosh end2 -15 -35.5 _sosh kn _knwall ks _kswall f _wfric
;wall type line3d end1 -20 35.5 _sosh end2 -20 -35.5 _sosh kn _knwall ks _kswall f _wfric
;wall type line3d end1 -25 35.5 _sosh end2 -25 -35.5 _sosh kn _knwall ks _kswall f _wfric
;wall type line3d end1 -30 35.5 _sosh end2 -30 -35.5 _sosh kn _knwall ks _kswall f _wfric
```

```
;wall type line3d end1 -35 35.5 _sosh end2 -35 -35.5 _sosh kn _knwall ks _kswall f _wfric
;wall type line3d end1 35.5 0 _sosh end2 -35.5 0 _sosh kn _knwall ks _kswall f _wfric
;wall type line3d end1 35.5 5 _sosh end2 -35.5 5 _sosh kn _knwall ks _kswall f _wfric
;wall type line3d end1 35.5 10 _sosh end2 -35.5 10 _sosh kn _knwall ks _kswall f _wfric
;wall type line3d end1 35.5 15 _sosh end2 -35.5 15 _sosh kn _knwall ks _kswall f _wfric
;wall type line3d end1 35.5 20 _sosh end2 -35.5 20 _sosh kn _knwall ks _kswall f _wfric
;wall type line3d end1 35.5 25 _sosh end2 -35.5 25 _sosh kn _knwall ks _kswall f _wfric
;wall type line3d end1 35.5 30 _sosh end2 -35.5 30 _sosh kn _knwall ks _kswall f _wfric
;wall type line3d end1 35.5 35 _sosh end2 -35.5 35 _sosh kn _knwall ks _kswall f _wfric
;wall type line3d end1 35.5 -5 _sosh end2 -35.5 -5 _sosh kn _knwall ks _kswall f _wfric
;wall type line3d end1 35.5 -10 _sosh end2 -35.5 -10 _sosh kn _knwall ks _kswall f _wfric
;wall type line3d end1 35.5 -15 _sosh end2 -35.5 -15 _sosh kn _knwall ks _kswall f _wfric
;wall type line3d end1 35.5 -20 _sosh end2 -35.5 -20 _sosh kn _knwall ks _kswall f _wfric
;wall type line3d end1 35.5 -25 _sosh end2 -35.5 -25 _sosh kn _knwall ks _kswall f _wfric
;wall type line3d end1 35.5 -30 _sosh end2 -35.5 -30 _sosh kn _knwall ks _kswall f _wfric
;wall type line3d end1 35.5 -35 _sosh end2 -35.5 -35 _sosh kn _knwall ks _kswall f _wfric

;.....................................................................
;Generate Ball
;.....................................................................
set gen_error off

generate x -70 70 y -70 70 z 1900 2500 rad 3 3 id 1 3500
prop dens _balldens kn _knball ks _ksball f _bfric

plot create 1
plot add ball y
plot add wall g wireframe on


;.....................................................................
;Measure porosity
;.....................................................................
measure id 1 x 0 y 0 z 35 radius 35
measure id 2 x 0 y 0 z 75 radius 35
measure id 3 x 0 y 0 z 115 radius 35
history id 1000 n 50 measure  p id=1
history id 1001 n 50 measure  p id=2
history id 1002 n 50 measure  p id=3

plot create poros1
plot add history 1000

plot create poros2
plot add history 1001

plot create poros3
plot add history 1002

;cycle 1000000

;delete wall 1000

;cycle 20000000

restore 3ftairpluv.sav

;pause
```

```
;.....................................................................
;Create Movie File
;.....................................................................
;set plot avi
;movie avi_open file movie_airpluviationsample3d_6mm.avi
;movie step 100 1 file movie_airpluviationsample3d_6mm.avi
;cycle 50000
;pause
;cycle 50000
;solve max 0.01
;movie avi_close file movie_airpluviationsample3d_6mm.avi



;.....................................................................
;Filename:  funnel_dep_6mm.dvr
;Author: Patrick Noble
;This Program generates a sample with use of the funnel deposition method.
;Note units are in m-kg-sec
;.....................................................................

set gravity 0 0 -9810

;.....................................................................
;Parameters FISH Function
;.....................................................................
define params
        _knwall = 500000000 ;wall normal stiffness
        _kswall = 500000000
        _knball = 202240  ;ball normall stiffness
        _ksball = 79000
        _wfric = 0.228 ;wall friction coefficient
        _bfric = 0.096 ;ball-ball friction coefficient
        _moldh = 150 ;mold height
        _moldr = 35.5 ;mold radius
        _platenr = _moldr + 3 ;base radius
        _tubeh = 200 ;tube length in mm
        _tuber = 12 ;tube radius
        _tubeend = _tubeh
        _funnelstart1 = _tubeh
        _funnelh1 = 200 ;funnel mouth height
        _funnelend1 = _funnelstart1 + _funnelh1
        _funnelr1 = 12 ;mouth radius
        _funnelr2 = 100 ;bowl radius
        _br = 3 ;ball radius
        _bv = (4*3.14159*(_br)^3)/3 ;ball volume
        _mv = _moldh*3.14159*(_moldr)^2 ;mold volume
        _targetporosity = 0.4
        _nb = _mv*_targetporosity/_bv ;number of balls to achieve desired porosity
        _nbg = _nb + 2000 ;number of balls to generate
        _balldens = 0.000007832 ;ball  density
        _genh1 = _funnelend2
        _genh2 = genh1 + 500
        _genb1 = _funnelr2*0.7
        _genb2 = -1*_genb1
end
params
```

```
;.....................................................................
;Generate walls for sample containment
;.....................................................................
wall type cylinder end1 0 0 0 end2 0 0 _moldh rad _moldr _moldr kn _knwall ks _kswall f _wfric
wall type disk rad _platenr norm 0 0 1 kn _knwall ks _kswall f _wfric

;.....................................................................
;Generate tube for funnel
;.....................................................................
wall type cylinder end1 0 0 0 end2 0 0 _tubeh rad _tuber _tuber kn _knwall ks _kswall f _wfric id 10000

;.....................................................................
;Generate Funnel
;.....................................................................
wall type cylinder end1 0 0 _tubeh end2 0 0 _funnelend1 rad _funnelr1 _funnelr2 kn _knwall ks _kswall f _wfric id
10001

generate x -70 70 y -70 70 z 500 1500 rad 3 3 id 1 3500
prop dens _balldens kn _knball ks _ksball f _bfric



plot create 1
plot add wall b wireframe on
plot add ball y

;.....................................................................
;Measure porosity
;.....................................................................
measure id 1 x 0 y 0 z 35 radius 35
measure id 2 x 0 y 0 z 75 radius 35
measure id 3 x 0 y 0 z 115 radius 35
history id 1000 n 50 measure  p id=1
history id 1001 n 50 measure  p id=2
history id 1002 n 50 measure  p id=3

plot create poros1
plot add history 1000

plot create poros2
plot add history 1001

plot create poros3
plot add history 1002

;.....................................................................
;Create Movie
;.....................................................................
;set plot avi
;movie avi_open file movie_funneldeptest.avi
;movie step 500 1 file movie_funneldeptest.avi

;movie avi_close file movie_airpluviationsample3d_6mm.avi
```

APPENDIX C

```
clear all
close all
clc

%%%%%%%%%%%%%%%%%%%%%%%%%%%%%%%%%%%%%%%%%%%%%%%%%%%%%%%%%%%%%%%%%%%%%%%%%%%%%%%
% Filename:  PFC_Void_Ratio.m
% Author:  Patrick Noble
% Date:  4-19-12
% This file reads an Excel spreadsheet of sphere position uploaded from
% PFC3D.  The void ratio of the sample along the sample height is generated
% as well as contour plots for the void ratio variation within the slice.
% TO generate the contour plot of a desired slice, change the length of
% slcht to the desired slice number.
%%%%%%%%%%%%%%%%%%%%%%%%%%%%%%%%%%%%%%%%%%%%%%%%%%%%%%%%%%%%%%%%%%%%%%%%%%%%%%%
tic

%Read Ball Position Spreadsheet
ballpos = xlsread('PFC3ftspherepositions1.xlsx');

%Cross sectional area of specimen
diam = 72;
rad = diam/2;
radpix = rad*7;
areapix = pi()*(radpix)^2;
slarea = pi()*rad^2;

%Void Ratio per Slice Height
slcht = 1:1:2;
for n = 1:length(slcht)
    count = n
    clear csarea
    clear r
    clear x
    clear y
    for i = 1:length(ballpos)
        if ballpos(i,4) <= slcht(n) + 3 && ballpos(i,4) >= slcht(n) - 3
            x(i) = ballpos(i,2) +50;
            y(i) = ballpos(i,3) +50;
            r(i) = sqrt(9 - (abs(ballpos(i,4)-slcht(n)))^2);
        end
    end
    for j = 1:length(x)
        csarea(j) = pi()*(r(j)^2);
    end
    spharea = sum(csarea);
    slvr(n) = (slarea-spharea)/spharea;
end

% avgpvr = mean(slvr);
% expermean = 0.632
% yp = 0:.1:136;
% % y2 = 0:.1:136;
% %
figure
hold
plot(slvr,slcht)
% plot(avgpvr,yp,'r')
```

```
% plot(expermean,yp,'g')
% legend('Planar Void Ratio','Average Planar Void Ratio','Experimental Void
Ratio','Location','East')
% title('PFC Sample Planar Void Ratio 3ft Drop Height')
% xlabel('Void Ratio')
% ylabel('Specimen Height (mm)')

%Draw Sphere Radius
InM = zeros(700,700);
theta = 0:1:360;
for j = 1:length(x)
    if x(j) > 0
        InM(round(y(j)*7),round(x(j)*7)) = 1;
        for k = 1:length(theta)
            xp = (r(j)*7-3)*cosd(theta(k));
            yp = (r(j)*7-3)*sind(theta(k));
            InM(round((y(j)*7)+yp),round((x(j)*7)+xp)) = 1;
        end
    else
    end
end

InI = mat2gray(InM);
BW = imfill(InI);
figure
imshow(BW)

%Generate "Filled Mold Image"
% se = strel('disk',25);
NM = zeros(700,700);
theta2 = 0:0.1:360;
for i = 1:length(theta2)
    xp2 = (175)*cosd(theta2(i));
    yp2 = (175)*sind(theta2(i));
    NM(round(350+yp2),round(350+xp2)) = 1;
end
NM = imfill(NM);

figure
imshow(NM)

%%%%%%%%%%%%%%%%%%%%%%%%%%%%%%%%%%%%%%%%%%%%%%%%%%%%%%%%%%%%%%%%%%%%%%%%%%%%%%%
%Variation of void ratio within slice
[dimy dimx c] = size(InM);

[X Y] = meshgrid(64:10:594,58:10:588);

InM = zeros(dimy,dimx);

%Control Area Dimensions
sqw = 5:15:110;
sqh = 5:15:110;

%Find Mesh Grid Points
pts = zeros(length(X)*length(Y),2);
pts(:,1) = X(:)';
pts(:,2) = Y(:)';

for n = 1:length(sqh)
    n = n
```

```
    for i = 1:length(pts)
        for j = 1:sqh(n)
            for k = 1:sqw(n)
                sqpx(j,k) = BW(round(pts(i,2) - sqh(n)/2 + j -1),...
                    round(pts(i,1) - sqw(n)/2 + k -1));
                contarea(j,k) = (NM(round(pts(i,2) - sqh(n)/2 + j -1),...
                    round(pts(i,1) - sqw(n)/2 + k -1)));
                 %Develop Matrix Showing Covered Area
%                 if n == 1
%                     InM(round(pts(i,2) - sqh(n)/2 + j -1),...
%                         round(pts(i,1) - sqw(n)/2 + k -1)) = 50;
%                 elseif n == 2
%                     InM(round(pts(i,2) - sqh(n)/2 + j -1),...
%                         round(pts(i,1) - sqw(n)/2 + k -1)) = 75;
%                 elseif n == 3
%                     InM(round(pts(i,2) - sqh(n)/2 + j -1),...
%                         round(pts(i,1) - sqw(n)/2 + k -1)) = 100;
%                 elseif n == 4
%                     InM(round(pts(i,2) - sqh(n)/2 + j -1),...
%                         round(pts(i,1) - sqw(n)/2 + k -1)) = 125;
%                 elseif n == 5
%                     InM(round(pts(i,2) - sqh(n)/2 + j -1),...
%                         round(pts(i,1) - sqw(n)/2 + k -1)) = 150;
%                 else
%                     InM(round(pts(i,2) - sqh(n)/2 + j -1),...
%                         round(pts(i,1) - sqw(n)/2 + k -1)) = 175;
%                 end
            end
        end
        areasphere = sum(sum(sqpx));
        areasq = sum(sum(contarea));
        %Void Ratio Calculation
        if areasq == 0
            vr(i) = 0;
        elseif areasq < 25
            vr(i) = 0;
        elseif areasq < 0.25*sqh(n)*sqw(n)
            vr(i) = 0;
        else
            vr(i) = (areasq - areasphere)/areasphere;
        end
    end
    %Void Ratio Matrix used for Contour plot
    VRT = vec2mat(vr,length(X));
    VRT = flipud(VRT');
    for ii = 1:length(X)
        for jj = 1:length(X)
            if VRT(ii,jj) > 1
                VRT(ii,jj) = 1;
            elseif VRT(ii,jj) < 0
                VRT(ii,jj) = 0;
            else
                VRT(ii,jj) = VRT(ii,jj);
            end
        end
    end
    %Calculate Void Ratio Statistics
    [r,c,v] = find(vr);
    meanvr(n,1) = mean(v);
    varvr(n,1) = var(v);
```

```
    sdvr(n,1) = sqrt(varvr(n,1));
    %Generate Contour Plot
    if n == length(sqh)
    figure
    contourf(X,Y,VRT,15);
    colorbar
    xlabel('Pixel Location')
    ylabel('Pixel Location')
%     titl = ['Void Ratio Contour Plot Slice 2' int2str(sqh(n)) 'x'
int2strg(sqh(n)) 'Control Area'];
%     title = (titl);
    else
    end
end

for i = 1:length(sqh)
    sqa(i) = sqh(i)*sqw(i);
end

gsphere = sum(sum(BW));
garea = 198180;
for i = 1:length(sqh)
    globalvr(i) = (garea-gsphere)/gsphere;
end

figure
hold
plot(sqa,meanvr)
scatter(sqa,meanvr,'filled','b')
% plot(sqa,globalvr,'r')
% legend('Mean Void Ratio','Slice Void Ratio')
xlabel('Control Area (Pixels^2)');
ylabel('Mean Void Ratio')

figure
hold
plot(sqa,sdvr)
scatter(sqa,sdvr,'filled','b')
xlabel('Control Area (Pixels^2)');
ylabel('Void Ratio Standarad Deviation');

% figure
% hold
% imshow(I)
% scatter(pts(:,1),pts(:,2),'r')


function [InId] = Local_Threshold(I,NoMold)

%%%%%%%%%%%%%%%%%%%%%%%%%%%%%%%%%%%%%%%%%%%%%%%%%%%%%%%%%%%%%%%%%%%%%%%%%%%%%%%
% Filename: Local_Threshold.m
% Author:  Patrick Noble
%
% This function file is used to create the local threshold binary
% image.  You must input the raw image (with out the mold) and a binary
% image (NoMold) where each pixel inside the mold is a one and each pixel
% outside is a zero.
%%%%%%%%%%%%%%%%%%%%%%%%%%%%%%%%%%%%%%%%%%%%%%%%%%%%%%%%%%%%%%%%%%%%%%%%%%%%%%%
```

```
[dimy dimx] = size(I);

for i = round(dimy/2)
    for j = 1:dimx
        xgray(j) = I(i,j);
    end
end

for j = round(dimx/2)
    for i = 1:dimy
        ygray(i) = I(i,j);
    end
end

xgray = single(uint8(xgray));
ygray = single(uint8(ygray));
bins = 0:10:250;

% figure
% hist(xgray(85:576),bins)
% title('Histogram of x-Profile Slice 132')
%
% figure
% hist(ygray(77:570),bins)
% title('Histogram of y-Profile Slice 132')

xgrayavg = smooth(xgray(83:571),251);
ygrayavg = smooth(ygray(80:566),251);

xx = 1:1:dimx;
xy = 1:1:dimy;

% figure
% plot(xx,xgray,xx(83:571),xgrayavg)
% title('x-Profile Slice 132')
% legend('Gray Scale Values','Moving Average');
%
% figure
% plot(xy,ygray,xy(80:566),ygrayavg)
% title('y-Profile Slice 132')
% legend('Gray Scale Values','Moving Average');
theta = 0:1:180;
centx = 329;
centy = 323;
radpx = 71.6*21;

for i = 1:dimy
    clear xgray
    clear xgrayavg
    clear xgrayavgind
    xgrayavg = single(uint8(zeros(dimx,1)));
    for j = 1:dimx
        xgray(j) = I(i,j);
        nmval(j) = ~NoMold(i,j);
    end
    xgray = single(uint8(xgray));
    if sum(nmval) == 0
        col(i) = 0;
        xgrayavg = smooth(xgray);
```

```
    else
        col = find(nmval == 1);
        xgrayavgind = smooth(xgray(col(1):col(length(col))),251);
        for k = col(1):length(col)+col(1)-1
            xgrayavg(k) = single(uint8(xgrayavgind(k-(col(1)-1))));
        end
    end
    for jj = 1:length(xgrayavg)
        if xgray(jj) > xgrayavg(jj)
            InMx(i,jj) = 250;
        else
            InMx(i,jj) = 0;
        end
    end
end
% trueavg = smooth(xgray(82:573),251);
% x = 1:1:dimx;
% figure
% plot(x,xgray,x,xgrayavg,x(82:573),trueavg)


InIx = mat2gray(InMx);

% se = strel('square',2);
% InIx = imopen(InIx,se);
% InIx = imclose(InIx,se);

% figure
% imshow(InIx)
% title('Local Threshold Image Slice 2 x')

for i = 1:dimx
    clear ygray
    clear ygrayavg
    clear ygrayavgind
    ygrayavg = single(uint8(zeros(dimy,1)));
    for j = 1:dimy
        ygray(j) = I(j,i);
        nmval(j) = ~NoMold(j,i);
    end
    ygray = single(uint8(ygray));
    if sum(nmval) == 0
        col(i) = 0;
        ygrayavg = smooth(ygray);
    else
        col = find(nmval == 1);
        ygrayavgind = smooth(ygray(col(1):col(length(col))),251);
        for k = col(1):length(col)+col(1)-1
            ygrayavg(k) = single(uint8(ygrayavgind(k-(col(1)-1))));
        end
    end
    for jj = 1:length(ygrayavg)
        if ygray(jj) > ygrayavg(jj)
            InMy(jj,i) = 250;
        else
            InMy(jj,i) = 0;
        end
    end
end
```

```
InIy = mat2gray(InMy);

% se = strel('square',2);
% InIy = imopen(InIy,se);
% InIy = imclose(InIy,se);



% figure
% imshow(InIy)
% title('Local Threshold Image Slice 2 y')

%Combine Ix and Iy
InI = zeros(dimy,dimx);

for i = 1:1:dimy
    for j = 1:1:dimx
        if InIx(i,j) == InIy(i,j)
            InI(i,j) = InIx(i,j);
        else
            InI(i,j) = 0;
        end
    end
end

% InI = bwmorph(InI,'majority');

% InI = imerode(InI,se);
% InI = imdilate(InI,se);

se = strel('square',2);
InId = imdilate(InI,se);

% figure
% imshow(InId)
% title('Local Threshold x plus y Slice 2 Dilate')

% BW = im2bw(I,thresh);
% figure
% imshow(BW)
% title('Global Threshold Image Slice 2')


end


function [spheres, multBW_close] = Remove_Mold(filename, thresh)

%%%%%%%%%%%%%%%%%%%%%%%%%%%%%%%%%%%%%%%%%%%%%%%%%%%%%%%%%%%%%%%%%%%%%%%%%%%%%%%
% Filename:  Remove_Mold.m
% Author:  Patrick Noble
% Date:  April 10th 2012
%
% Note:  This file was adapted from imaging_microtomograph_f.m written by
% Zenon Medina-Cetina.
%
% Function use:
% Remove_Mold.m reads an image file and removes the exterior mold and
% outlying noise from a CT scan image of a granular sample.  The input for
```

```
% the function is a string containing the name of the file to be read and
% the threshold value of the objects to keep. The image file must be in the
% same folder as this function.  The function output is the resulting
% image. Input images should be of type uint8.  The output image will also
% be uint8.  The Output Image No_Mold shows the total area contained within
% the mold.
%
% Code Example:
%
% filename = ['image.tif'];
% thresh = .6
% [Crop_Image, No_Mold] = Remove_Mold(filename, thresh);
%%%%%%%%%%%%%%%%%%%%%%%%%%%%%%%%%%%%%%%%%%%%%%%%%%%%%%%%%%%%%%%%%%%%%%%%%%%


I = imread(filename);
% thresh = 140/255;
BW = im2bw(I,thresh);

se = strel('disk',25);
BW_close = imclose(BW,se);

% figure
% imshow(BW_close)

% se2 = strel('square',6)
% BW_close_open = imopen(BW,se2);
% figure
% imshow(BW_close_open)

Isize = size(BW)
for row = round(Isize(2)/2)
    for col = 1:round(Isize(1)/2)
        if BW(row,col),
            break
        end
    end

    connectivity = 8;

    mold = bwtraceboundary(BW_close, [row, col], 'NE', connectivity);
    % border.ext = mold;
end

% figure
% imshow(I)
% hold
% plot(mold(:,2),mold(:,1),'r');

invBW = ~BW_close;
multBW_close = immultiply(uint8(invBW),255);
% figure;
% imshow(multBW_close)


spheres = imsubtract(I,multBW_close);

% figure
% imshow(spheres)
```

```
return


clear all
close all
clc

%%%%%%%%%%%%%%%%%%%%%%%%%%%%%%%%%%%%%%%%%%%%%%%%%%%%%%%%%%%%%%%%%%%%%%%%%%%%%%%
% Filename:  Void_Ratio_Variability3.m
% Author:  Patrick Noble
%
% This file crates the void ratio contour plots for the CT scan images.
% Function files Remove_Mold and Local_Threshold are required to prepare
% the image and generate the binary image required for this analysis.
%%%%%%%%%%%%%%%%%%%%%%%%%%%%%%%%%%%%%%%%%%%%%%%%%%%%%%%%%%%%%%%%%%%%%%%%%%%%%%%


tic

filename = ['Crop Not Modified66.tif'];
thresh = 140/255;

[I, NM] = Remove_Mold(filename, thresh);

[dimy dimx c] = size(I);

[X Y] = meshgrid(64:10:594,58:10:588);

[BW] = Local_Threshold(I,NM);

InM = zeros(dimy,dimx);

%Control Area Dimensions
sqw = 5:15:110;
sqh = 5:15:110;

%Find Mesh Grid Points
pts = zeros(length(X)*length(Y),2);
pts(:,1) = X(:)';
pts(:,2) = Y(:)';

for n = 1:length(sqh)
    n = n
    for i = 1:length(pts)
        for j = 1:sqh(n)
            for k = 1:sqw(n)
                sqpx(j,k) = BW(round(pts(i,2) - sqh(n)/2 + j -1),...
                    round(pts(i,1) - sqw(n)/2 + k -1));
                contarea(j,k) = (~NM(round(pts(i,2) - sqh(n)/2 + j -1),...
                    round(pts(i,1) - sqw(n)/2 + k -1)));
                 %Develop Matrix Showing Covered Area
%                 if n == 1
%                     InM(round(pts(i,2) - sqh(n)/2 + j -1),...
%                         round(pts(i,1) - sqw(n)/2 + k -1)) = 50;
%                 elseif n == 2
%                     InM(round(pts(i,2) - sqh(n)/2 + j -1),...
%                         round(pts(i,1) - sqw(n)/2 + k -1)) = 75;
%                 elseif n == 3
%                     InM(round(pts(i,2) - sqh(n)/2 + j -1),...
```

```
%                       round(pts(i,1) - sqw(n)/2 + k -1)) = 100;
%                 elseif n == 4
%                     InM(round(pts(i,2) - sqh(n)/2 + j -1),...
%                       round(pts(i,1) - sqw(n)/2 + k -1)) = 125;
%                 elseif n == 5
%                     InM(round(pts(i,2) - sqh(n)/2 + j -1),...
%                       round(pts(i,1) - sqw(n)/2 + k -1)) = 150;
%                 else
%                     InM(round(pts(i,2) - sqh(n)/2 + j -1),...
%                       round(pts(i,1) - sqw(n)/2 + k -1)) = 175;
%                 end
            end
        end
        areasphere = sum(sum(sqpx));
        areasq = sum(sum(contarea));
        %Void Ratio Calculation
        if areasq == 0
            vr(i) = 0;
        elseif areasq < 25
            vr(i) = 0;
        elseif areasq < 0.25*sqh(n)*sqw(n)
            vr(i) = 0;
        else
            vr(i) = (areasq - areasphere)/areasphere;
        end
    end
    %Void Ratio Matrix used for Contour plot
    VRT = vec2mat(vr,length(X));
    VRT = flipud(VRT');
    for ii = 1:length(X)
        for jj = 1:length(X)
            if VRT(ii,jj) > 1
                VRT(ii,jj) = 1;
            elseif VRT(ii,jj) < 0
                VRT(ii,jj) = 0;
            else
                VRT(ii,jj) = VRT(ii,jj);
            end
        end
    end
    %Calculate Void Ratio Statistics
    [r,c,v] = find(vr);
    meanvr(n,1) = mean(v);
    varvr(n,1) = var(v);
    sdvr(n,1) = sqrt(varvr(n,1));
    %Generate Contour Plot
    if n == length(sqh)
    figure
    contourf(X,Y,VRT,15);
    colorbar
    xlabel('Pixel Location')
    ylabel('Pixel Location')
%     titl = ['Void Ratio Contour Plot Slice 2' int2str(sqh(n)) 'x'
int2strg(sqh(n)) 'Control Area'];
%     title = (titl);
    else
    end
end

for i = 1:length(sqh)
```

```
    sqa(i) = sqh(i)*sqw(i);
end

gsphere = sum(sum(BW));
garea = 198180;
for i = 1:length(sqh)
    globalvr(i) = (garea-gsphere)/gsphere;
end

figure
hold
plot(sqa,meanvr)
scatter(sqa,meanvr,'filled','b')
% plot(sqa,globalvr,'r')
% legend('Mean Void Ratio','Slice Void Ratio')
xlabel('Control Area (Pixels^2)');
ylabel('Mean Void Ratio')

figure
hold
plot(sqa,sdvr)
scatter(sqa,sdvr,'filled','b')
xlabel('Control Area (Pixels^2)');
ylabel('Void Ratio Standarad Deviation');

% figure
% hold
% imshow(I)
% scatter(pts(:,1),pts(:,2),'r')


toc


clear all
close all
clc

%%%%%%%%%%%%%%%%%%%%%%%%%%%%%%%%%%%%%%%%%%%%%%%%%%%%%%%%%%%%%%%%%%%%%%%%%%%%%%%
% Filename:  Profile_Derivatives.m
% Author:  Patrick Noble
%
% This file create a binary image using the second derivative method.
% The function Remove-Mold is required to prepare the image.
%
%%%%%%%%%%%%%%%%%%%%%%%%%%%%%%%%%%%%%%%%%%%%%%%%%%%%%%%%%%%%%%%%%%%%%%%%%%%%%%%
tic
%Vector of number of slices used in imagecompilerfunc
numpic = 1:1:133;

%Run imagecompilerfunc to assemble slices into a 3D Matrix
% [I3D os os2] = imagecompilerfunc(numpic);

%Read Image File
% I = imread('Crop Not Modified2.tif');
% figure;
% imshow(I)
% title('Image of Slice 2')
```

```
%Load Image and Remove Mold
filename =['Crop Not Modified2.tif'];
thresh = 140/255;
[Ix] = Remove_Mold(filename,thresh);
[Iy] = Remove_Mold(filename,thresh);
J = imread(filename);
%Traditional threshold image
thresh = 140/255;
BWt = im2bw(Ix,thresh);
% figure;
% imshow(BWt)
% title('Traditional Threshold Image Slice 2')
%Deblur image
% PSF = fspecial('gaussian',7,10);
% DB = deconvlucy(I,PSF);

% Perform Opening by Reconstruction to smooth Image.
se = strel('disk',3);
Iex = imerode(Ix,se);
Ix = imreconstruct(Iex,Ix);
Iey = imerode(Iy,se);
Iy = imreconstruct(Iey,Iy);
% figure;
% imshow(Iobr)
% title('Opening by Reconstruction')



[dimy dimx] = size(Ix)

for i = 1:dimy
    for j = 1:dimx
        xgray(j) = Ix(i,j);
    end
    xgray = int32(xgray);
    xgray = single(xgray);
    xgrayavg = smooth(xgray,11);
    dxgray = zeros(dimx-1,1);
    ddxgray = zeros(dimx-2,1);
    for ii = 2:length(xgrayavg)-1
        dxgray(ii-1) = (xgrayavg(ii+1)-xgrayavg(ii-1))/2;
    end
    for ii = 2:length(dxgray)-1
        ddxgray(ii-1) = (xgrayavg(ii+1)-2*xgrayavg(ii)+xgrayavg(ii-1));
    end
    for k = 2:length(ddxgray)-1
        if ddxgray(k-1) < 0 && ddxgray(k) < 0 && ddxgray(k+1) < 0
%             DB(i,k) = uint8(255);
            Ix(i,k) = uint8(255);
            sphval(k) = 255;
            sphpts(k) = k;
        elseif dxgray(k-1) > dxgray(k) && dxgray(k) > dxgray(k+1)
%             DB(i,k) = uint8(255);
            Ix(i,k) = uint8(255);
        elseif ddxgray(k) < 0
%             DB(i,k) = uint8(255);
            Ix(i,k) = uint8(255);
        else
%             DB(i,k) = uint8(0);
            Ix(i,k) = uint8(0);
```

```
            sphval(k) = 0;
            sphpts(k) = 0;
        end
    end
end

for i = 1:dimx
    for j = 1:dimy
        ygray(j) = Iy(j,i);
    end
    ygray = int32(ygray);
    ygray = single(ygray);
    ygrayavg = smooth(ygray,11);
    dygray = zeros(dimy-1,1);
    ddygray = zeros(dimy-2,1);
    for ii = 2:length(ygrayavg)-1
        dygray(ii-1) = (ygrayavg(ii+1)-ygrayavg(ii-1))/2;
    end
    for ii = 2:length(dygray)-1
        ddygray(ii-1) = (ygrayavg(ii+1)-2*ygrayavg(ii)+ygrayavg(ii-1));
    end
    for k = 2:length(ddygray)-1
        if ddygray(k-1) < 0 && ddygray(k) < 0 && ddygray(k+1) < 0
%             DB(i,k) = uint8(255);
            Iy(k,i) = uint8(255);
            sphval(k) = 255;
            sphpts(k) = k;
        elseif dygray(k-1) > dygray(k) && dygray(k) > dygray(k+1)
%             DB(i,k) = uint8(255);
            Iy(k,i) = uint8(255);
        elseif ddygray(k) < 0
%             DB(i,k) = uint8(255);
            Iy(k,i) = uint8(255);
        else
%             DB(i,k) = uint8(0);
            Iy(k,i) = uint8(0);
            sphval(k) = 0;
            sphpts(k) = 0;
        end
    end
end



x = 1:1:dimx;
dx = 1:length(dxgray);
ddx = 2:1:length(ddxgray)+1;
% for i = 1:length(inflptsx)
%     yv(i) = 0;
%     yinf(i) = round(dimy/2);
% end

% figure;
% plot(dx,dxgray)
% hold
% scatter(inflptsx,yv,'r')
% title('First Derivative')

% figure;
% plot(x,xgray);
```

```
% hold
% plot(x,xgrayavg,'r');

% figure;
% imshow(J)
% hold on
% % plot(ddx,ddxgray,'g');
% scatter(inflptsx,yinf,'b')
% % plot(x,round(dimy/2))

% figure;
% plot(ddx,ddxgray)
% hold
% scatter(inflptsx,yv,'r')
% title('Second Derivative')

% for i = 1:length(sphpts)
%     ypts(i) = round(dimy/2);
% end
% figure;
% imshow(I)
% hold
% scatter(sphpts,ypts)

figure
imshow(Ix)
title('Reconstructed Image From Derivatives x')

se = strel('square',3);
Ixc = imclose(Ix,se);
Ixco = imopen(Ixc,se);

% figure
% imshow(Ixco)
% title('After Close and Open x')

figure
imshow(Iy)
title('Reconstructed Image From Derivatives y')

se = strel('square',3);
Iyc = imclose(Iy,se);
Iyco = imopen(Iyc,se);

% figure
% imshow(Iyco)
% title('After Close and Open y')

%Combine Ix and Iy
InI = zeros(dimy,dimx);

for i = 1:1:dimy
    for j = 1:1:dimx
        if Ixco(i,j) == Iyco(i,j)
            InI(i,j) = Ixco(i,j);
        else
            InI(i,j) = 0;
        end
    end
end
```

```
figure
imshow(InI)
title('Ix plus Iy')

se3 = strel('square',4);
InIc = imclose(InI,se3);
InIco = imopen(InIc,se3);
% figure
% imshow(InIco)
% title('Ix plus Iy After Close Open')

% figure
% imshow(BWt)
% title('Traditional Threshold Image')

se2 = strel('square',2)
BWtc = imclose(BWt,se2);
BWtco = imopen(BWtc,se2);

% figure
% imshow(BWtco)
% title('Traditional After Close and Open')

% for i = 1:dimx
%     for j = 1:round(dimy/2)
%         Jn(j,i) = uint8(InI(j,i));
%     end
%     for j = round(dimy/2):dimy
%         Jn(j,i) = J(j,i);
%     end
% end
%
% figure
% imshow(Jn)
%
% for i = 1:dimy
%     for j = 1:round(dimx/2)
%         Jn2(i,j) = uint8(InI(i,j));
%     end
%     for j = round(dimx/2):dimx
%         Jn2(i,j) = J(i,j);
%     end
% end
%
% figure
% imshow(Jn2)
%
%
% %%%%%%%%%%%%%%%%%%%%%%%%%%%%%%%%%%%%%%%%%%%%%%%%%%%%%%%%%%%%%%%%%%%%%%%%%%%
% %Fit Circles to Combine Derivative Image
%     %Gather Image Statistics
%     [B, L] = bwboundaries(InIco);
%     numRegions = max(L(:));
%     %imshow(label2rgb(L))
%     stats = regionprops(L,'all');
%     Area = [stats.Area];
%     minor = [stats.MinorAxisLength];
%     major = [stats.MajorAxisLength];
%     centroids = [stats.Centroid]';
```

```
%     keep = find(major<=21);
%     discard = find(major>21);
%
%     for j=1:length(keep)
%         outline = B{keep(j)};
%         line(outline(:,2),outline(:,1),'color','r','linewidth',1)
%     end
%
%     %Find centroid location of spheres to keep
%     centcount = 1:2:length(centroids);
%     for i = 1:length(centcount)
%         centroidy(i,1) = round(centroids(centcount(i)));
%         centroidx(i,1) = round(centroids(centcount(i)+1));
%     end
%     for i = 1:length(keep)
%         centroidykeep(i) = centroidy(keep(i));
%         centroidxkeep(i) = centroidx(keep(i));
%     end
%
%     %Find radii of spheres to keep
%     for i = 1:length(keep)
%         radii(i) = round((minor(keep(i))+major(keep(i)))/4)-1;
%     end
%
%     %Generate Image with only kept spheres
%     NewImg2 = zeros(dimy,dimx);
%     for i = 1:length(keep)
%         theta = 0:1:360;
%         for j = 1:length(theta)
%             x = radii(i)*cos(theta(j));
%             y = radii(i)*sin(theta(j));
%             NewImg2(round(centroidxkeep(i)+x),round(centroidykeep(i)+y))...
%                 = 1;
%         end
%     end
%
%     NI3= mat2gray(NewImg2);
%     Repro2 = im2bw(NI3);
%     Repro2 = imfill(Repro2,'holes');
%     figure
%     imshow(Repro2)



% figure
% imshow(DB)


clear all
close all
clc

%%%%%%%%%%%%%%%%%%%%%%%%%%%%%%%%%%%%%%%%%%%%%%%%%%%%%%%%%%%%%%%%%%%%%%%%%%%%%%%
% Filename:  Planar_Void_Ratio.m
% % Author:  Patrick Noble
%
% This file generate planar void ratio plots for the CT scan images.
% The function files Remove_mold and Local_Threshold are required to
% prepare the image and create the binary image used to calculate
```

```
% the void ratio.
%
%%%%%%%%%%%%%%%%%%%%%%%%%%%%%%%%%%%%%%%%%%%%%%%%%%%%%%%%%%%%%%%%%%%%%%%%%%%%%%%
tic
%Vector of number of slices used in imagecompilerfunc
numpic = 1:1:133;

%Run imagecompilerfunc to assemble slices into a 3D Matrix
% [I3D os os2] = imagecompilerfunc(numpic);

%Initialize planar void ratio vector
pvr = zeros(1,length(numpic));

%cross sectional area of specimen
diam = 71.76;
rad = diam/2;
radpix = rad*7;
areapix = pi()*(radpix)^2;

for i = 1:length(numpic)
    %Read Image file
    filename = ['Crop Not Modified' int2str(i) '.tif']
    %Set Threshold limit
    thresh = 140/255;
    %Remove Image exterior and mold
    [I NM] = Remove_Mold(filename, thresh);
    [BW] = Local_Threshold(I,NM);
    %Convert to binary
%     BW = im2bw(I,thresh);
%     se = strel('square',2);
%     BWc = imclose(BW,se);
%     BWco = imopen(BWc,se);
    %Find area of spheres
    areasph(i) = sum(sum(BW));
    pvr(i) = (areapix - areasph(i))/areasph(i);
end

% figure
% imshow(BW)
% figure
% imshow(BWc)
% figure
% imshow(BWco)

avgpvr = mean(pvr);
expermean = 0.580
y = 0:.1:133;
y2 = 0:.1:133;

figure;
hold
plot(pvr,numpic,'b')
plot(avgpvr,y,'color','r')
plot(expermean,y2,'color','g')
legend('Planar Void Ratio','Mean Planar Void Ratio',...
    'Experimental Global Void Ratio','Location','SouthEast')
title('Planar Void Ratio vs Height of sample')
xlabel('Void Ratio')
ylabel('Specimen Height (mm)')
toc
```

```
function [I3D os os2] = imagecompilerfunc(numpic)

%%%%%%%%%%%%%%%%%%%%%%%%%%%%%%%%%%%%%%%%%%%%%%%%%%%%%%%%%%%%%%%%%%%%%%%%%%%%%%%
% Filename:  Image_Compiler.m
% Author:  Patrick Noble
% Date:  3-21-12
%
% Program Function:  This program compiles images of slices taken from a CT
% scan and compiles the image information into a single 3D Matrix.  This
% file must be saved in the same place as the sequence of Images.  All
% image names must not contain any characters before the slice number.
% For example CropBinary1.tif is an acceptable file name, however
% CropBinary0001.tif is unacceptable.  A slice of the 3D matrix can be
% obtained by changing the k value in the loop under Generate Slice of
% 3D Image.  The index k corresponds to the x value of the pixel location
% in the 2D image.  A Slice can be obtained in an orthogonal direction by
% switching j and k in the following manner: OS1(i,j)=I3D(k,j,sliceht(i)).
% The index j must also be changed to vary with x.  This is achieved
% by changing the condition statement in the for loop to:
% j = 1:length(indexx).
% NOTE:  Ensure that the strings in filename and imread match the names
%   associated with the file and file type (ie. *.tif, *.bmp, *.png, etc.).
%
% Input:
% numpic = A vector that contains the number of each slice.
%
% Output:
% I3D = A 3D Matrix of all the slices.
% os = An image showing a slice through the center the sample perpendicular
%     to the x-axis.
% os2 = An image showing a slice through the center of the sample
%     perpendicular to the y-axis.
%%%%%%%%%%%%%%%%%%%%%%%%%%%%%%%%%%%%%%%%%%%%%%%%%%%%%%%%%%%%%%%%%%%%%%%%%%%%%%%

%Vector of the number of images
%numpic = 1:1:133;

%Determine Size of 3D Matrix
IS = imread('Crop Not Modified1.tif');
ISize = size(IS);
indexx = zeros(ISize(2),1);
indexy = zeros(ISize(1),1);
I3D = zeros(ISize(1),ISize(2),length(numpic));

for i = 1:length(numpic)
    filename = ['Crop Not Modified' int2str(i) '.tif']
    I = imread(filename);
    I3D(:,:,i) = I;
end

%Generate Slice of 3D Image Perdendicular to the x-axis
sliceht = max(numpic):-1:1;
for i = 1:(length(numpic))
    for j = 1:length(indexy)
        for k = round(ISize(2)/2)
            OS1(i,j) = I3D(j,k,sliceht(i));
        end
```

```
    end
end

%Generate Slice of 3D Image Perpendicular to the y-axis
sliceht = max(numpic):-1:1;
for i = 1:(length(numpic)-1)
    for j = 1:length(indexx)
        for k = round(ISize(1)/2)
            OS2(i,j) = I3D(k,j,sliceht(i));
        end
    end
end

os = mat2gray(OS1);
% %OrthoSlice = im2bw(os);
% figure;
% imshow(os)
% title('Orthogonal Slice Through Specimen Perpendicular to x-axis');
%
os2 = mat2gray(OS2);
% %OrthoSlice = im2bw(os2);
% figure;
% imshow(os2)
% title('Orthogonal Slice Through Specimen Perpendicular to y-axis');

return
```

VITA

Name:	Patrick Russell Noble
Address:	10205 Westheimer Rd #100 Houston, TX 77042
Email Address:	patrick.noble12@gmail.com
Education:	B.S., Civil Engineering, Texas A&M University, 2010 M.S., Structural Engineering, Texas A&M University, 2012